Circ J 2003; **67:** 354–356

Congenitally Corrected Transposition of the Great Arteries Treated by Partial Systemic Ventriculectomy

Ayaka Kobashi, MD; Michihiro Suwa, MD, Tomomi Nakamura, MD; Takahide Ito, MD; Taiko Horii, MD*; Tadashi Isomura, MD*; Hisayoshi Suma, MD*

Congenitally corrected transposition of the great arteries (CCTGA) is a rare congenital heart disease characterized by atrioventricular (AV) and ventriculo-arterial discordance;[1] that is, the left ventricle supports the pulmonary circulation and the right ventricle supports the systemic circulation. The most common cardiac anomalies in CCTGA include ventricular septal defect, pulmonary outflow tract obstruction and abnormalities of the systemic AV valve! The dysfunction of the systemic ventricle occurs with increasing frequency in older patients with CCTGA, independent of their commonly associated structural defects[2–4] We report a patient with CCTGA undergone the partial ventriculectomy for his systemic ventricular dysfunction. (*Circ J* 2003; **67:** 354–356)

Key Words: Corrected transposition of the great arteries; Partial left ventriculectomy; Partial systemic ventriculectomy

A 42-year-old man was admitted to hospital with worsening dyspnea. At the age of 18, he underwent annuloplasty of the systemic AV valve for severe valvular regurgitation related to CCTGA at another hospital and did not have any problems on follow-up until age 33 when he visited hospital with paroxysmal nocturnal dyspnea. Because the systemic AV valve regurgitation had recurred to a severe degree and systemic ventricular contraction had decreased, he underwent systemic AV valve replacement and annuloplasty of the pulmonary AV valve. At age 39, atrial fibrillation with a rapid heart rate developed and could not be controlled with medications, so the His-bundle was cryoablated to block AV conduction and a permanent rate-adaptive pacemaker inserted intravenously. Although he was controlled in all pacemaker rhythm without tachycardia, his systemic ventricular function decreased and he was in New York Heart Association (NYHA) functional class 4 even after receiving digitalis, diuretics, angiotensin-converting enzyme inhibitor (ACEI) and other oral inotropic agents.

His height was 185 cm and body weight was 75 kg. His blood pressure was 116/60 mmHg and the pulse rate was 60 beats/min and regular. Auscultation showed no significant murmur. Electrocardiograms revealed all pacemaker rhythm (VVI). Chest X-rays showed a cardiothoracic ratio of 58% and systemic atrial and ventricular enlargement. Echocardiography revealed enlargement of the systemic atrium and ventricle, and reduction of the systemic ventricular systolic function (the left atrial dimension was 4.7 cm, the end-diastolic dimension of the systemic ventricle was 8.6 cm and the fractional shortening was 14%) (Table 1, Fig 1). Pulmonary wedge pressure and right-side pressures were elevated (Table 2). The systemic ventriculogram showed diffused hypokinesis, but myocardial perfusion imaging using technetium-99m tetrofosmin indicated a severe perfusion defect in the lateral wall and the apex at rest.

Because his symptoms could not be relieved by medical treatment, he was transferred to Shonan Kamakura General Hospital to undergo partial systemic ventriculectomy in February 1998. Under cardiopulmonary bypass (CPB) with heart beating and without aortic cross-clamping, the systemic ventricle was incised laterally from the apex to the base. There was neither mitral apparatus nor recognizable papillary muscle because of the previous valve replacement. Much of the anterolateral wall that was thin and akinetic on intraoperative palpation, and which corresponded to the defect on perfusion imaging, was excised in a tear-drop shape (7 cm wide and 12 cm long, 66 g in weight). Closure of the ventricle was done in 2 layers. The duration of CPB was 73 min and ventricular function recovered well without mechanical support. The resected myocardium had severe interstitial fibrosis (28.5%) and mild degeneration and hypertrophy of the myocardial cells.

On echocardiography, the end-diastolic dimension of the systemic ventricle decreased to 5.7 cm, but the ejection fraction (EF) had not changed at 1 month after the operation (Table 1, Fig 1). A thickened pericardium and pericardial effusion were noted behind the systemic ventricle after the operation. On contrast-enhanced electron-beam computed tomograms, the end-diastolic volume of the systemic ventricle was decreased from 213 ml to 180 ml after systemic ventriculectomy, but stroke volume was not reduced (38 ml to 41 ml) and the EF increased from 18% to 23% (Table 2). On cardiac catheterization performed 2 months after the operation, pulmonary wedge pressure and right-side pressures were decreased, but cardiac output (CO) was somewhat reduced (Table 2). Nine months after the operation, CO returned to the preoperative level (Table 2) and the EF had increased from 15% to 38% on radionuclide angiography (Table 3), but pulmonary wedge pressure and right-side pressures were re-elevated (Table 2).

The patient's symptoms had clearly improved after the

(Received June 25, 2001; revised manuscript received January 17, 2002; accepted January 22, 2002)

*The Third Division, Department of Internal Medicine, Osaka Medical College, Takatsuki and *Department of Cardiovascular Surgery, Hayama Heart Center, Kanagawa, Japan*

Mailing address: Michihiro Suwa, MD, The Third Division, Department of Internal Medicine, Osaka Medical College, 2-7 Daigaku-cho, Takatsuki City, Osaka 569-8686-MZ, Japan. E-mail: in3028@poh.osaka-med.ac.jp

Table 1 Echocardiographic Data

	Oct. 97	Mar. 98	Nov. 98	Aug. 99	Aug. 01
LAD (cm)	4.7	4.6	4.9	4.9	5.0
Dd (cm)	8.6	5.7	6.5	5.7	5.8
Ds (cm)	7.4	4.9	5.5	4.7	4.7
IVS (cm)	0.6	1.0	1.2	1.2	1.1
PW (cm)	1.1	1.0	0.9	0.9	0.9
FS (%)	14	14	15	18	20
EF (%)	29	30	32	37	40
	Before*	1 month**	9 months**	18 months**	42 months**

LAD, left atrial dimension; Dd, end-diastolic dimension of the systemic ventricle; Ds, end-systolic dimension of the systemic ventricle; IVS, thickness of interventricular septum in end-diastole; PW, posterior wall thickness of the systemic ventricle in end-diastole; FS, fractional shortening; EF, ejection fraction.
**Before partial ventriculectomy; **Months after partial ventriculectomy.*

operation, but he is still in NYHA functional class 3 and receiving diuretics and ACEI. The pulmonary artery and pulmonary capillary wedge pressures gradually rose to the preoperative levels, although the systemic ventricle had not dilated 26-42 months after the operation. The EF calculated by echocardiogram had improved after the operation, but it is questionable whether a one-dimensional observation is accurate.

Discussion

In CCTGA, the dysfunction of the systemic ventricle occurs with increasing frequency in older patients;[2–4] Graham et al[4] reported long-term outcomes of 182 patients with CCTGA, which indicated that by age 45, 56% of the patients with associated lesions had moderate or severe systemic ventricular dysfunction, and 32% of the patients without associated lesions had this complication. They also reported that the strongest risk factors for clinical congestive heart failure and systemic ventricular dysfunction were systemic valve surgery, systemic AV valve regurgitation, significant arrhythmia, history of any open heart surgery, and pacemaker therapy. However, it remains speculative whether systemic AV valve regurgitation is a causative or a secondary complication of systemic ventricular dysfunction?[3–5] The present patient had all these risk factors and when he underwent systemic AV valve replacement for the severe valve regurgitation, his systemic ventricular contraction had already decreased (Table 3). Open heart surgery (particularly systemic AV valve surgery) is associated with the progression of systemic ventricular dysfunction and probably results from an increase in afterload and/or difficulty in myocardial protection during surgery[4] The further reduction of the systemic ventricular EF after systemic AV valve replacement in this patient is possibly the result of increased afterload related to the correction of AV valve regurgitation (Table 3). Heart block and ventricular pacing can worsen systemic ventricular dysfunction because they can result in discordant ventricular contraction[4]

It is considered that long-term exposure to systemic pressure is an etiology of systemic ventricular dysfunction in patients with CCTGA? Hornung et al detected myocardial perfusion defects on radioisotope images in 5 patients with CCTGA who had not undergone surgery[6] Fixed defects that suggested myocardial infarction were seen in all 5 and reversible myocardial ischemia was present in 4 of them. Irreversible defects were mostly associated with the impairment of wall motion, and the EF was decreased in 4 patients. It is now clear that the coronary flow supplied

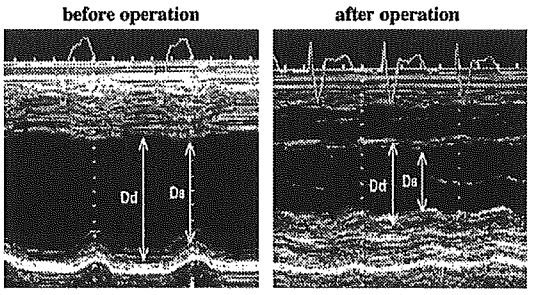

Fig 1. M-mode echocardiography performed before (Left) and 1 month after (Right) partial ventriculectomy. The end-diastolic dimension of the systemic ventricle decreased from 8.6 cm to 5.7 cm, but the calculated fractional shortening did not change. After the operation, an echo-free space, suspected to be a hemorrhagic pericardial effusion, and thickened pericardium were seen behind the systemic ventricle.

by only the right coronary artery system to a markedly dilated systemic ventricle is inadequate for myocardial perfusion.

Batista recently introduced a new procedure for patients with a very dilated and poorly contracting left ventricle resulting from any etiology, in which a large wedge of left ventricular myocardium is removed? The principle underlying this partial left ventriculectomy is related to LaPlace's law; that is, to reduce the wall tension by shortening the diameter of the left ventricle. Batista reported 120 surgical patients with 30-day mortality rates of 22% and 2-year survival rates of 55%. Most of the surviving patients improved from NYHA functional class 4 to either class 1 (57%) or 2 (33%). In Japan, cardiac transplantation has recently begun, but there is a shortage of donors, so since 1996 partial left ventriculectomy has been performed as a treatment for patients with end-stage dilated cardiomyopathy in Japan[8] Starling et al indicated that although stroke volume is reduced after ventriculectomy, the heart rate increases, and the end result is somewhat increased CO. However, they suggested that this procedure gave only temporary improvement in clinical compensation because the CO fell back to baseline levels after 3-12 months in spite of the increase of stroke volume? The current indications and efficacy of partial left ventriculectomy for advanced heart failure in patients with dilated cardiomyopathy are controversial[9,10]

Because the systemic ventricle was markedly dilated in the present patient, and the lateral segment had a myocardial perfusion defect, we considered that systolic function

Table 2 Cardiac Catheterization Data

	May. 97	*Apr. 98*	*Nov. 98*	*Apr. 00*
RA (mmHg)	*(7)*	*(6)*	*(11)*	*(8)*
Pul.V (mmHg)	*40/~8*	*29/~7*		*44/~7*
PA (mmHg)	*37/18 (24)*	*26/12 (18)*	*40/20 (32)*	*45/20 (31)*
PCW (mmHg)	*(19)*	*(12)*	*(19)*	*(17)*
Sys.V (mmHg)	*105/~14*	*81/~12*	*98/~20*	*96/~19*
Ao (mmHg)	*105/70 (80)*	*80/55 (62)*	*100/70 (82)*	*102/70 (88)*
CO (L/min)	*5.63*	*4.50*	*5.46*	*5.37*
CI ($L \cdot min^{-1} \cdot m^{-2}$)	*2.84*	*2.36*	*2.71*	*2.70*
EDV (ml)§	*[261.3]*	*163.3*	*230.7*	*201.8*
ESV (ml)§	*[232.8]*	*101.5*	*144.1*	*156.9*
SV (ml)§	*[28.5]*	*61.9*	*86.6*	*44.9*
EF (%)§	*[11]*	*38*	*38*	*22*
EDV (ml)¶	*213*	*180*		
ESV (ml)¶	*175*	*139*		
SV (ml)¶	*38*	*41*		
EF (%)¶	*18*	*23*		
	*before**	*2 months***	*9 months***	*26 months***

RA, right atrium; Pul.V, pulmonary ventricle; PA, pulmonary artery; PCW, pulmonary capillary wedge; Sys.V, systemic ventricle; Ao, aorta; CO, cardiac output (by thermodilution method); CI, cardiac index; EDV, end-diastolic volume; ESV, end-systolic volume; SV, stroke volume; EF, ejection fraction.
**Before partial ventriculectomy; **Months after partial ventriculectomy.*
CO and CI were measured by thermodilution method.
§Obtained from ventriculogram; ¶Obtained from electron-beam computed tomography.
[ ] data not reliable because of poor imaging on ventriculogram.

Table 3 Radionuclide Angiographic Data

	Before volume reduction			*After volume reduction*
	*Dec. 87**	*Feb. 88*	*April. 97*	*Nov. 98***
EF of Sys. V (%)	*51*	*37*	*15*	*38*
EF of Pul. V (%)	*77*	*91*	*70*	*59*

EF, ejection fraction; Sys.V, systemic ventricle; Pul.V, pulmonary ventricle.
**1 month after systemic AV valve replacement; **9 months after partial ventriculectomy.*

could be improved by reducing the volume of the systemic ventricle, particularly by removing the fibrous segment as in aneurysmectomy. Recent reports indicate that mitral valve surgery can rescue patients with heart failure who have a dilated and poorly contracting left ventricle accompanied by moderate to severe mitral regurgitation,[10] but we considered that mitral replacement would not provide relief for this patient because he had already undergone that treatment 9 years before.

After operation, the pulmonary artery and pulmonary capillary pressures gradually rose to the preoperative level. Although there was no sign that the systemic ventricle had dilated again, its systolic function had clearly deteriorated after the partial systemic ventriculectomy and we could not clarify why the EF obtained with echocardiography conflicted with the value obtained from catheterization. These changes may relate to systemic ventricular dysfunction that persists after the operation, restrictive physiology because of volume reduction and constrictive physiology related to the three pericardiotomies. Finally, although we could not conclude how the patient's symptoms had been relieved, we consider that partial systemic ventriculectomy can be effective, but not curative, for patients with CCTGA and heart failure.

References

1. Freedom RM, Dyck JD. Congenitally corrected transposition of the great arteries. *In:* Emmamouilides GC, Allen HD, Riemenschneider TA, Gutgesell HP, editors. Moss and Adams Heart disease in infants, children, and adolescents including the fetus and young adult. Baltimore: Williams & Wilkins; 1995: 1225–1245.
2. Graham TP Jr, Parrish MD, Boucek RJ Jr, Boerth RC, Breitweser JA, Thompson S, et al. Assessment of ventricular size and function in congenitally corrected transposition of the great arteries. *Am J Cardiol* 1983; **51:** 244–251.
3. Presbitero P, Somerville J, Rabajoli F, Stone S, Conte MR. Corrected transposition of the great arteries without associated defects in adult patients: Clinical profile and follow up. *Br Heart J* 1995; **74:** 57–59.
4. Graham TP Jr, Bernard YD, Mellen BG, Celermajer D, Baumgartner H, Cetta F, et al. Long-term outcome in congenitally corrected transposition of the great arteries. *J Am Coll Cardiol* 2000; **36:** 255–261.
5. Connelly MS, Liu PP, Williams WG, Webb GD, Robertson P, McLaughlin PR. Congenitally corrected transposition of the great arteries in the adult: Functional status and complications. *J Am Coll Cardiol* 1996; **27:** 1238–1243.
6. Hornung TS, Bernard EJ, Jaeggi ET, Howman-Giles RB, Celermajer DS, Hawker RE. Myocardial perfusion defects and associated systemic ventricular dysfunction in congenitally corrected transposition of the great arteries. *Heart* 1998; **80:** 322–326.
7. Batista RJ, Verde J, Nery P, Bocchino L, Takeshita N, Bhayana JN, et al. Partial left ventriculectomy to treat end-stage heart disease. *Ann Thorac Surg* 1997; **64:** 634–638.
8. Suma H, Horii T, Ichihara T, Hisamochi K, Takuma S, Iwahashi K. New surgical procedure for patients with dilated heart and end-stage cardiac failure (Batista procedure). *J Cardiol* 1997; **29:** 117–122.
9. Starling RC, McCarthy PM, Buda T, Wong J, Goormastic M, Smedira NG, et al. Results of partial left ventriculectomy for dilated cardiomyopathy: Hemodynamic, clinical and echocardiographic observations. *J Am Coll Cardiol* 2000; **36:** 2098–2103.
10. Suma H, Isomura T, Horii T, Sato T, Kikuchi N, Iwahashi K, et al. Nontransplant cardiac surgery for end-stage cardiomyopathy. *J Thorac Cardiovasc Surg* 2000; **119:** 1233–1244.

[CANCER RESEARCH 63, 8629–8633, December 15, 2003]

An Opposing View on WWOX Protein Function as a Tumor Suppressor

Akira Watanabe,[1] Yoshitaka Hippo,[1] Hirokazu Taniguchi,[1] Hiroko Iwanari,[3] Masakazu Yashiro,[4] Kosei Hirakawa,[4] Tatsuhiko Kodama,[2] and Hiroyuki Aburatani[1]

[1]Genome Science Division and [2]Laboratory of Systems Biology and Medicine, Research Center for Advanced Science and Technology, The University of Tokyo, Tokyo; [3]Perseus Proteomics, Inc., Tokyo; and [4]First Department of Surgery, Osaka City University Medical School, Osaka, Japan

ABSTRACT

WW domain-containing oxidoreductase (*WWOX*) is a candidate tumor suppressor gene. Because mutation or deletion in the coding region of *WWOX* is rarely found, it is speculated that the appearance of aberrant transcripts affects progression of various cancers. However, little is known about the role in these cancers of the WWOX protein. To characterize endogenous WWOX proteins, we analyzed WWOX expression using newly generated monoclonal antibodies. In immunoblot analysis of 49 cancer cell lines, only the normal form of the protein was detectable, although some of cell lines exhibited aberrant *WWOX* RNA transcripts. Accumulation of truncated proteins was observed by inhibiting proteasomal degradation with MG-132, whereas expression level of normal protein did not change, suggesting truncated proteins may be subjected to rapid degradation through proteasomal machinery. Immunohistochemistry for cancer cells demonstrated that WWOX protein levels are not decreased but rather elevated in gastric and breast carcinoma, challenging the notion of WWOX as a classical tumor suppressor. In noncancerous cells, WWOX was observed only in epithelial cells, including hormone-regulated cells such as Leydig cells, follicular cells, prostate epithelium, and mammary glands. Interestingly, restricted staining in nuclei was observed in some mammary gland cells while other epithelial cells exhibited localization of WWOX in cytoplasm. Nuclear localization of WWOX was also confirmed in confluent human fibroblast KMS-6, whereas WWOX was associated mainly with mitochondria before reaching confluence, indicating that WWOX shuttles between cytoplasm and nuclei. These findings provide novel insights into aspects of human WWOX function in both normal and malignant cells.

INTRODUCTION

Common fragile sites can contribute to oncogenesis by facilitating gene inactivation through chromosomal deletion or amplification (1). The common fragile site *FRA16D* on chromosome 16q23.3-24.2 is localized within a large region of chromosomal instability in cancers defined by loss of heterozygosity (2–5) and homozygous deletion (6, 7). Mashimo *et al.* (8) reported that microcell-mediated chromosome transfer of chromosome 16q23-24 resulted in strong suppression of metastatic activity in prostatic cancer cell lines, indicating the presence of a major tumor suppressor gene associated with cancer progression on 16q23.3-24.2.

WW domain-containing oxidoreductase (*WWOX*) was cloned from this *FRA16D* site (9, 10). From its deduced amino acid sequence, two functional domains were predicted; the first, at the NH_2 terminus, is a tandem WW domain that is likely to be involved in protein-protein interactions. The second is short-chain dehydrogenase/reductase domain that is shared in common among metabolic enzymes of steroid hormones (11). On the basis of the function of these motifs and the observation that *WWOX* shows elevated expression in hormonally regulated tissues such as testis, prostate, and ovary, it has been speculated that WWOX is functionally related to steroid hormones (9).

WWOX is reported to behave aberrantly in cancers of the breast, ovary, esophagus, and lung (9, 12–16). Although truncated *WWOX* transcripts are frequently observed in cancers from these tissues, mutations or deletions of the gene in the coding region are rarely found. Ectopic expression of WWOX protein induces apoptosis (11) and suppression of tumor growth both *in vitro* and *in vivo* (17). From these findings, *WWOX* was proposed to be a candidate tumor suppressor gene in which the function is presumably inactivated by the dominant negative action of truncated products from aberrant transcripts (17). However, a consistent picture of the subcellular localization of WWOX has not yet emerged (11, 17), and the dominant negative theory of WWOX action has remained untested without direct examination of endogenous expression of WWOX protein. Consequently, little is known about the role of WWOX protein in cancer progression.

To address these issues, we performed immunoblotting, subcellular localization analysis, and immunohistochemistry using newly generated monoclonal antibodies and provide new insights into the molecular understanding of WWOX protein in normal and cancer cells.

MATERIALS AND METHODS

Tumor Cell Lines. The stomach cancer cell lines OCUM-2M, OCUM-2MD3, and OCUM-2MLN were previously established by Yashiro *et al.* (18) and Fujiwara *et al.* (19). An additional 46 tumor cell lines derived from different tumor types (stomach, liver, lung, colon, esophagus, pancreas, kidney, brain, and breast) were obtained from the American Type Culture Collection (Manassas, VA), Riken Cell Bank (Tsukuba, Japan), Cell Resource Center for Biomedical Research at Tohoku University (Sendai, Japan), and Japanese Collection of Research Bioresources (Tokyo, Japan). Human skin fibroblast KMS-6 was purchased from Dainippon Pharmaceutical Co. Ltd. (Osaka, Japan)

Reverse Transcription-PCR and Northern Blot Analysis. cDNA derived from human *WWOX* was synthesized with oligodeoxythymidylic acid primer from 1 μg of total RNA and diluted up to 80 μl as described previously (20). Reverse transcription-PCR was performed with Advantage cDNA polymerase mixture (Clontech, Palo Alto, CA) and 1 μl of cDNA for 1 cycle of 94°C for 2 min, followed by 35 cycles of 94°C for 30 s, 63°C for 30 s, and 68°C for 3 min. Primers for amplification of sequence from exon 1 to 9 were 5′-GTGCCTCCACAGTCAGCCATG-3′ (sense) and 5′-CATCCCTCCCAGACCCTCCAGT-3′ (antisense). Glyceraldehyde-3-phosphate dehydrogenase primers were CATGTGGGCCATGAGGTCCACCAC (sense) and AATGCCTCCTGCACCACCAACTGC (antisense). Northern blot analysis and quantification of mRNA expression, using 20 μg of total RNA encoding normal *WWOX*, was performed as described previously (20).

Generation of Anti-WWOX Monoclonal Antibodies. A glutathione *S*-transferase-fusion protein of human WWOX derived from normal tissue was constructed in the expression vector pET 41 (Novagen, Madison, WI). Fusion proteins were induced in BL-21 Codon Plus (DE3; Stratagene, La Jolla, CA)

Received 4/18/03; revised 9/16/03; accepted 9/29/03.

Grant support: Grants-in-Aid for Scientific Research (B) 12557051 and 13218019 and Scientific Research on Priority Areas (C) 12217031 from Ministry of Education, Culture, Sports, Science and Technology (H. A.). This study was carried out as a part of The Technology Development for Analysis of Protein Expression and Interaction in Bioconsortia on R&D of New Industrial Science and Technology Frontiers which was supported by Industrial Science, Technology and Environmental, Policy Bureau, Ministry of Economy, Trade and Industry and delegated to New Energy Development Organization.

The costs of publication of this article were defrayed in part by the payment of page charges. This article must therefore be hereby marked *advertisement* in accordance with 18 U.S.C. Section 1734 solely to indicate this fact.

Note: Drs. Watanabe and Hippo contributed equally to this study.

Requests for reprints: Hiroyuki Aburatani, Genome Science Division, Research Center for Advanced Science and Technology, The University of Tokyo, 4-6-1, Komaba, Meguro-ku, Tokyo 153-8904, Japan. Phone: 81-3-5452-5352; Fax: 81-3-5452-5355; E-mail: haburata-tky@umin.ac.jp.

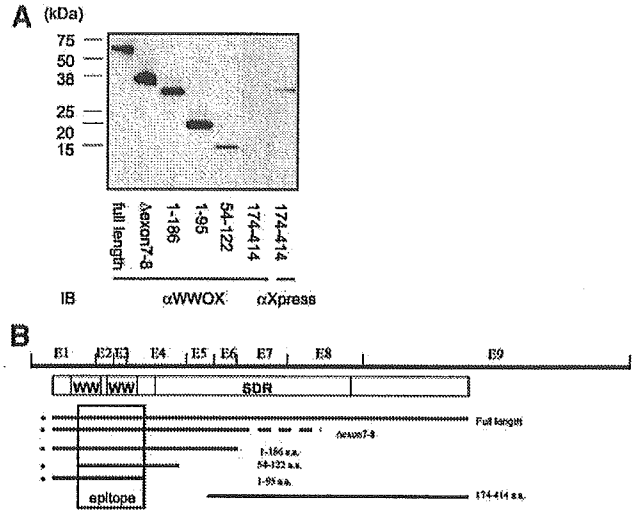

Fig. 1. Epitope mapping of anti-WWOX monoclonal antibody H2267. *A*, immunoblot analysis was performed with anti-WWOX antibody H2267 (*Lanes 1–6*) and anti-Xpress antibody (*Lane 7*). Xpress-tagged proteins were obtained by transfection of expression vector with inserts into COS7 cells. *B*, a schematic representation of various recombinant WWOX proteins, *asterisk marked bars* indicate the deduced region where the epitope of antibody H2267 resides.

and purified using Glutathione Sepharose 4B (Amersham Biosciences, Uppsala, Sweden) according to the manufacture's instructions. Recombinant glutathione *S*-transferase-WWOX was used for 3 cycles of immunization against female BALB/c mice. Spleen cells were isolated and fused with NS-1 myeloma cells (Dainippon Pharmaceutical Co., Ltd.). Hybridomas were selected by ELISA against the purified recombinant glutathione *S*-transferase-fused WWOX. After ELISA against glutathione *S*-transferase-WWOX, 90 hybridoma clones were selected and purified by limited dilution. For mass production, 7 clones of hybridomas were grown in mice ascites. Ascite fluids were collected and purified using ammonium sulfate.

Epitope Mapping. To obtain an antibody that recognizes both normal full-length and truncated proteins, we determined the epitope of each antibody by immunoblotting with recombinant normal and truncated WWOX proteins to correspond to amino acids 1–186, 1–98, amino acids 54–122, amino acids 171–414, and Δexon7–8 inserted into expression vector pcDNA4/HisMax (Invitrogen, Carlsbad, CA). Expression vectors with inserts were transfected into COS-7 using FuGENE 6 Transfection Reagent (Roche, Mannheim, Germany). Recombinant WWOX proteins containing the NH_2-terminal leader peptide Xpress epitope were obtained 2 days after transfection, and expression of proteins were confirmed by immunoblotting with anti-Xpress antibody (Invitrogen) and antimouse IgG antibody according to the following procedure.

Immunoblot Analysis. Proteins (10 μg) were resolved on 12% SDS-PAGE and transferred to polyvinylidene difluoride membranes (Hybond-P; Amersham Biosciences, Piscataway, NJ). After blocking the membranes with 2% nonfat milk in PBS for 1 h, immunoblotting was performed with an anti-WWOX antibody H2267 as primary antibody. Peroxidase-conjugated antimouse IgG antibody (Amersham Biosciences) was used as secondary antibody, and ECL-PLUS Detection System (Amersham Biosciences) was used as substrate for chemiluminescent detection. Quantification of WWOX protein level was performed on a Densitograph Lane and Spot Analyzer (Atto, Tokyo, Japan). To examine rapid degradation of truncated proteins, an inhibition of proteasomal machinery assay was performed using the proteasome inhibitor MG-132, obtained from the Peptide Institute (Osaka, Japan). A total of 5 μM MG-132 dissolved in DMSO or DMSO only was used to treat HCT-116 cells for 10 h, followed by immunoblot analysis.

Immunohistochemical Analysis. Immunohistochemical analysis was performed against samples from a formalin-fixed, paraffin embedded tissue archive. Tissue collection and the subsequent study had full local research ethics approval. The sections were deparaffinised in xylene, washed in ethanol, and rehydrated in Tris-buffered saline. Antigen retrieval was performed in 10 mM citrate buffer pH 7.0 at 120°C for 10 min, followed by incubation with 2% nonfat milk in Tris-buffered saline. Sections were then incubated an antibody H2267 (50 μg/ml) for 1 h, followed by secondary staining with Dako Envision+ (Dako Ltd., Cambridge, United Kingdom). All sections were counter stained with Mayer's hematoxylin.

Subcellular Localization Analysis. Immunostaining of culture cells were performed after fixation in 4% paraformaldehyde and permeabilization in 0.2% Triton X-100 followed by incubation with 2% nonfat milk in Tris-buffered saline. To gain higher, an antibody in immunostaining were biotinylated by reacting antibodies with *N*-hydroxysuccinimide biotin. A biotinylated antibody H2267-biotin (50 μg/ml) was applied as primary antibody for 1 h and FITC-labeled Avidin (Vector Laboratories, Inc., Burlingame, CA) was used as secondary reagent. Dual-color detection by confocal laser scan microscopy was performed after treatment with a 0.5 μM solution of the mitochondrial stain MitoTracker Red CMXRos (Molecular Probes, Inc., Eugene, OR).

RESULTS

Generation and Characterization of Monoclonal Antibodies against Human WWOX. We established 90 clones of hybridoma producing antihuman WWOX antibodies. To select antibodies that can recognize both normal and truncated proteins, we performed epitope mapping for antibodies from 7 clones. Antibody H2267 recognized a region within amino acids 54–98 (Fig. 1*A*). All truncated WWOX proteins with Δexon 5–8, Δexon 6–8 and a novel isoform Δexon7–8, described below in this study, possess amino acids 1–136. Thus, antibody H2267 can recognize both normal and truncated WWOX proteins and was selected for use in the following study.

Expression Analysis of WWOX Transcripts and Proteins in Cancer Cell Lines. We examined the expression of *WWOX* by reverse transcription-PCR in 49 cancer cell lines derived from stomach, liver, lung, colon, esophagus, pancreas, kidney, brain, and breast. Except for the gastric cancer cell line MKN7 that lacks full-length transcripts containing exons 1–9, all of the 48 remaining cell lines expressed full-length transcripts containing exons 1–9. In addition to full-length transcripts, aberrant transcripts were found in OCUM-2MD3, SCH, AGS, LoVo, HCT-116, Capan-1, and MCF-7 (Fig. 2*A*). Sequence analysis of these transcripts revealed a novel aberrant transcript in OCUM-2MD3 and HLE in which alternative splicing resulted in the absence of exons 7–8.

Next, we examined the expression of WWOX proteins in cancer cells by immunoblot analysis. We anticipated the presence of truncated proteins corresponding to the aberrant transcripts identified in

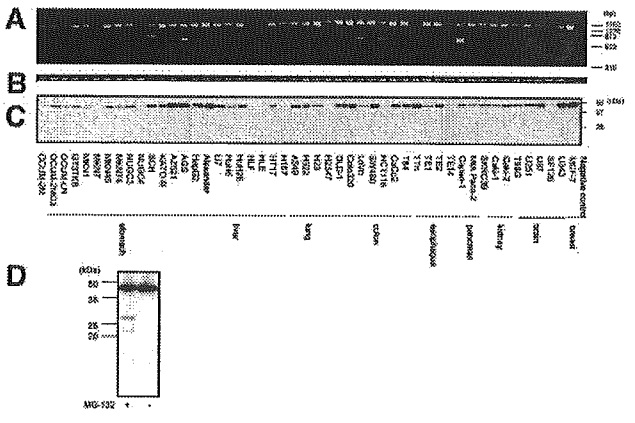

Fig. 2. Expression of *WWOX* transcripts and proteins in cancer cell lines. *A*, reverse transcription-PCR for amplification of fragments containing exons 1–9 of *WWOX*. *B*, reverse transcription-PCR for *GAPDH* as an internal control. *C*, immunoblot analysis of WWOX using anti-WWOX antibody H2267. Note only normal WWOX protein was detected. *D*, proteasome inhibitor MG-132 (5 μM) induced accumulation of truncated protein of WWOX in HCT-116 cells. + and − indicates with or without MG-132, respectively.

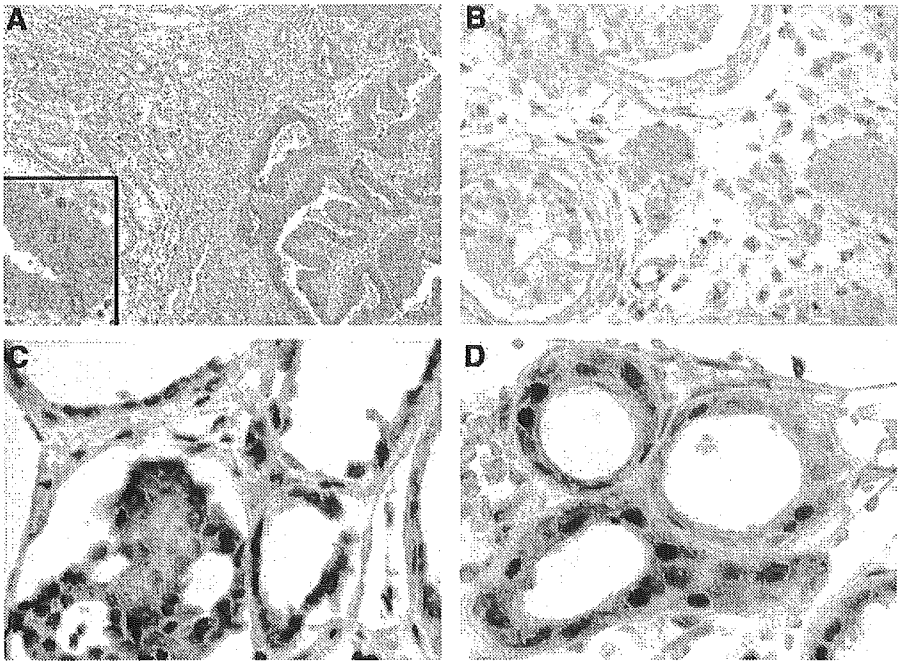

Fig. 3. Immunohistochemical analysis of WWOX. *A*, strong staining is observed in gastric cancer cell (*right* and *inset*), but only weak staining in normal epithelium (*top left*) and no staining in intestinal metaplasia (*bottom left*) was observed in gastric cancer tissue (×100). Magnification is shown in *inset* (×400). *B*, strong staining in Leydig cells (*center*) and weak staining in testicular epithelium is observed in testis (×200). *C*, strong staining in follicular epithelium was observed in thyroid (×400). *D*, restricted nuclear staining is observed in some cells, whereas most cells showed reactivity in cytoplasm in mammary glands (×400).

seven of the cell lines. However, truncated proteins of M_r 35,000 for Δexon5–8, M_r 26,100 for Δexon 6–8, and M_r 35,200 for Δexon7–8, that would correspond to the truncated *WWOX* mRNA transcripts could not be identified in any of the seven cell lines. The 48 cell lines, except for MKN7, expressed a normal WWOX protein (Fig. 2*C*).

Mechanism for Truncated WWOX Protein Absence. We next investigated the reason why truncated products from aberrant transcripts were not detected by immunoblotting. We first suspected that the small amount of aberrant transcripts in cell lines was undetectable: Even in cells with a relatively large amount of aberrant transcripts such as Capan-1 and MCF7, the quantitative ratio of aberrant to normal transcripts determined by Northern blotting was 0.63 and 0.069, respectively. However, truncated proteins could readily be detected in HCT-116 cells treated with the proteasome inhibitor MG-132 (Fig. 2*D*), whereas expression levels of normal WWOX remained unchanged, suggesting that truncated WWOX proteins are not usually detectable due to rapid and selective degradation.

Immunohistochemistry in Tumor and Normal Tissues. To describe WWOX expression *in vivo*, immunohistochemical analysis was performed. If WWOX is a tumor suppressor, decreased expression may be expected in cancer. However, strong staining in cytoplasm was unexpectedly observed in 10 of 16 cases of gastric carcinoma (Fig. 3*A*) and 5 of 5 cases of breast carcinoma (data not shown), whereas staining in surrounding noncancerous cells was weak. In normal tissues, staining was observed only in epithelial cells, particularly in hormone-regulated organs such as testis (Fig. 3*B*), thyroid (Fig. 3*C*), prostate, and mammary glands, consistent with the previous analysis by Northern blotting (9) and our Gene Expression Database by oligonucleotide microarray.[5] In testis, WWOX was enriched in Leydig cells, which are known to produce testosterones (Fig. 3*B*). Interestingly, staining in nucleus was observed in mammary epithelia (Fig. 3*D*), whereas other epithelial cells were stained in the cytoplasm (Fig. 3, *A–C*).

Subcellular Localization Analysis in Culture Cells. Subcellular localization of endogenous WWOX in cultured cells was determined by confocal laser scan microscopy analysis. Dual-color detection of WWOX and mitochondria demonstrated that localization of WWOX was mainly to mitochondria (Fig. 4, *A–C*). However, as shown in Fig. 4*D*, WWOX translocates into nuclei under confluent culture conditions.

DISCUSSION

The present study is an extension of our initial goal of identifying tumor suppressor loci in gastric cancer. We had searched for genomic homozygous deletions in the highly metastatic schirrous gastric cancer cell line OCUM-2MD3 using representational differential analysis with isogenic gastric fibroblast as a reference. This analysis identified several homozygously deleted fragments of ~300bp, including fragments mapped in 3p14 and 16q23, latterly identified as intronic region of *fragile histidine triad* at *FRA3B* and *WWOX* at *FRA16D*, respectively. Both fragments were deleted during malignant progression to OCUM-2MD3 from OCUM-2M, a poorly metastatic and isogenic ancestral line of OCUM-2MD3. As well as *fragile histidine triad*, alterations in *WWOX* such as rare point mutations and frequent intronic deletions and expression of aberrant transcripts found in gastric cancers (unpublished results). Prompted by these notable similarities of *WWOX* to *fragile histidine triad*, which now established as a tumor suppressor after a long period of controversy (21), we set out to analyze WWOX at the protein level.

To make sure of WWOX as a tumor suppressor, the following two points are needed: (*a*) whether protein expression of WWOX in cancer declines; and (*b*) what impact of aberrant transcripts in cancer has (17). To verify these issues, we focused on chasing a fate of aberrant transcripts and making protein expression in cancer clear by immunohistochemistry.

By immunoblotting with an antibody, which can recognize both full-length and truncated WWOX, we were not able to detect truncated proteins and only detected normal WWOX proteins from cell lines, which expressed normal and truncated RNA transcripts. Truncated proteins were not detectable under physiological condition until proteasomal inhibitor MG-132 was treated(Fig. 2*D*). These observa-

[5] http://www2.genome.rcast.u-tokyo.ac.jp/database/.

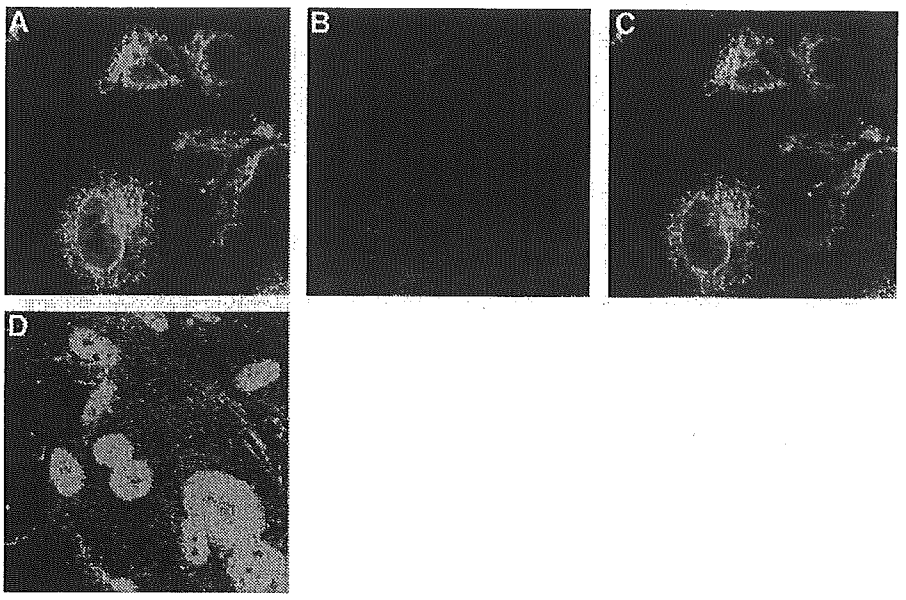

Fig. 4. Subcellular localization of WWOX in human skin fibroblast KMS-6 cells by laser confocal microscopy. *A*, WWOX protein stained with anti-WWOX antibody A2267. *B*, mitochondria stained with MitoTracker Red CMXRos. *C*, merged image demonstrates localization of endogenous WWOX protein in mitochondria. *D*, WWOX translocates into nucleus in KMS-6 under confluent culture conditions.

tions indicate that truncated WWOX proteins in cancer are unstable and subject to rapid proteasomal degradation and contradicts the possibility that truncated WWOX proteins acts in a dominant negative manner. On account of the possibility that mutated WWOX acts in the dominant negative manner, we examined sequence analysis in the coding region. Cancer-specific missense mutations in coding region were not found in 49 cell lines examined, although polymorphism, which were identified in normal individuals, were found in these cell lines (data not shown). This result is consistent to a report by Paige *et al.* (12), indicating that cancer progression is rarely caused by mutation of WWOX.

Our immunohistochemical analysis in most specimens examined showed expression of WWOX in cancer cells is rather elevated by comparison with that in noncancerous cells. Therefore, we did not find predicted evidences of WWOX as a tumor suppressor. Aberrant transcripts of *WWOX* could be produced as a result of chromosomal instability in 16q23.3-24.2 region, where another tumor suppressor gene might reside. Thus, at present, we cannot conclude that WWOX is a tumor suppressor.

We next examined localization of WWOX protein. A consistent picture of the subcellular localization of WWOX has yet to emerge: localization of ectopic WWOX in Golgi apparatus was observed by Bednarek *et al.* (17), whereas Chang *et al.* (11) reported that endogenous WWOX is localized in mitochondria and translocated to nuclei after tumor necrosis factor α stimulation. The discrepancy between two previous studies in the subcellular localization of WWOX may be caused by the difference between endogenous and ectopic expression. We confirmed that intrinsic WWOX localizes mainly in mitochondria and translocates into nuclei under confluent culture conditions. Because nuclear localization of WWOX was also detected *in vivo*, this translocation may be relevant to its function. Our observations are consistent with the report by Chang *et al.*, who demonstrated interaction of WWOX with p53 (11) and phosphorylation of Tyr^{33} within WW domain by c-Jun NH_2-terminal kinase 1 (22). Shifting of WWOX localization may be controlled by phosphorylation of tyrosine within the WW domain.

In summary, to our knowledge, this is the first article describing expression of WWOX protein in cancers. Our results show there is little possibility that aberrant transcripts in cancer cells behave in a dominant negative fashion. Besides, immunohistochemical analysis in this study was not able to detect down-regulation of WWOX protein in cancer. Thus, our result by protein expression analysis using specific antibody did not support WWOX as a tumor suppressor. Additional characterization of WWOX protein such as mechanism of WWOX translocation will be required to elucidate its function.

ACKNOWLEDGMENTS

We gratefully acknowledge Drs. Shuichi Tsutsumi, Shumpei Ishikawa, and Eiji Warabi for useful comments, Saori Fukui for protein expression, and Erio Ashihara-Fujita for cell culture.

REFERENCES

1. Sutherland, G. R., Baker, E., and Richards, R. I. Fragile sites still breaking. Trends Genet., *14:* 501–506, 1998.
2. Suzuki, H., Komiya, A., Emi, M., Kuramochi, H., Shiraishi, T., Yatani, R., and Shimazaki, J. Three distinct commonly deleted regions of chromosome arm 16q in human primary and metastatic prostate cancers. Genes Chromosomes Cancer, *17:* 225–233, 1996.
3. Driouch, K., Dorion-Bonnet, F., Briffod, M., Champeme, M. H., Longy, M., and Lidereau, R. Loss of heterozygosity on chromosome arm 16q in breast cancer metastases. Genes Chromosomes Cancer, *19:* 185–191, 1997.
4. Chen, T., Sahin, A., and Aldaz, C. M. Deletion map of chromosome 16q in ductal carcinoma *in situ* of the breast: refining a putative tumor suppressor gene region. Cancer Res., *56:* 5605–5609, 1996.
5. Li, C., Berx, G., Larsson, C., Auer, G., Aspenblad, U., Pan, Y., Sundelin, B., Ekman, P., Nordenskjold, M., van Roy, F., and Bergerheim, U. S. Distinct deleted regions on chromosome segment 16q23-24 associated with metastases in prostate cancer. Genes Chromosomes Cancer, *24:* 175–182, 1999.
6. Paige, A. J., Taylor, K. J., Stewart, A., Sgouros, J. G., Gabra, H., Sellar, G. C., Smyth, J. F., Porteous, D. J., and Watson, J. E. A 700-kb physical map of a region of 16q23.2 homozygously deleted in multiple cancers and spanning the common fragile site FRA16D. Cancer Res., *60:* 1690–1697, 2000.
7. Krummel, K. A., Roberts, L. R., Kawakami, M., Glover, T. W., and Smith, D. I. The characterization of the common fragile site FRA16D and its involvement in multiple myeloma translocations. Genomics, *69:* 37–46, 2000.
8. Mashimo, T., Watabe, M., Cuthbert, A. P., Newbold, R. F., Rinker-Schaeffer, C. W., Helfer, E., and Watabe, K. Human chromosome 16 suppresses metastasis but not tumorigenesis in rat prostatic tumor cells. Cancer Res., *58:* 4572–4576, 1998.
9. Bednarek, A. K., Laflin, K. J., Daniel, R. L., Liao, Q., Hawkins, K. A., and Aldaz, C. M. WWOX, a novel WW domain-containing protein mapping to human chromosome 16q23.3-24.1, a region frequently affected in breast cancer. Cancer Res., *60:* 2140–2145, 2000.
10. Ried, K., Finnis, M., Hobson, L., Mangelsdorf, M., Dayan, S., Nancarrow, J. K., Woollatt, E., Kremmidiotis, G., Gardner, A., Venter, D., Baker, E., and Richards, R. I. Common chromosomal fragile site FRA16D sequence: identification of the FOR gene

spanning FRA16D and homozygous deletions and translocation breakpoints in cancer cells. Hum. Mol. Genet., *9:* 1651–1663, 2000.
11. Chang, N. S., Pratt, N., Heath, J., Schultz, L., Sleve, D., Carey, G. B., and Zevotek, N. Hyaluronidase induction of a WW domain-containing oxidoreductase that enhances tumor necrosis factor cytotoxicity. J. Biol. Chem., *276:* 3361–3370, 2001.
12. Paige, A. J., Taylor, K. J., Taylor, C., Hillier, S. G., Farrington, S., Scott, D., Porteous, D. J., Smyth, J. F., Gabra, H., and Watson, J. E. WWOX: a candidate tumor suppressor gene involved in multiple tumor types. Proc. Natl. Acad. Sci. USA, *98:* 11417–11422, 2001.
13. Driouch, K., Prydz, H., Monese, R., Johansen, H., Lidereau, R., and Frengen, E. Alternative transcripts of the candidate tumor suppressor gene, WWOX, are expressed at high levels in human breast tumors. Oncogene, *21:* 1832–1840, 2002.
14. Kuroki, T., Trapasso, F., Shiraishi, T., Alder, H., Mimori, K., Mori, M., and Croce, C. M. Genetic alterations of the tumor suppressor gene WWOX in esophageal squamous cell carcinoma. Cancer Res., *62:* 2258–2260, 2002.
15. Yakicier, M. C., Legoix, P., Vaury, C., Gressin, L., Tubacher, E., Capron, F., Bayer, J., Degott, C., Balabaud, C., and Zucman-Rossi, J. Identification of homozygous deletions at chromosome 16q23 in aflatoxin B1 exposed hepatocellular carcinoma. Oncogene, *20:* 5232–5238, 2001.
16. Yendamuri, S., Kuroki, T., Trapasso, F., Henry, A. C., Dumon, K. R., Huebner, K., Williams, N. N., Kaiser, L. R., and Croce, C. M. WW domain containing oxidoreductase gene expression is altered in non-small cell lung cancer. Cancer Res., *63:* 878–881, 2003.
17. Bednarek, A. K., Keck-Waggoner, C. L., Daniel, R. L., Laflin, K. J., Bergsagel, P. L., Kiguchi, K., Brenner, A. J., and Aldaz, C. M. WWOX, the *FRA16D* gene, behaves as a suppressor of tumor growth. Cancer Res., *61:* 8068–8073, 2001.
18. Yashiro, M., Chung, Y. S., Nishimura, S., Inoue, T., and Sowa, M. Peritoneal metastatic model for human scirrhous gastric carcinoma in nude mice. Clin. Exp. Metastasis, *14:* 43–54, 1996.
19. Fujihara, T., Sawada, T., Hirakawa, K., Chung, Y. S., Yashiro, M., Inoue, T., and Sowa, M. Establishment of lymph node metastatic model for human gastric cancer in nude mice and analysis of factors associated with metastasis. Clin. Exp. Metastasis, *16:* 389–398, 1998.
20. Hippo, Y., Yashiro, M., Ishii, M., Taniguchi, H., Tsutsumi, S., Hirakawa, K., Kodama, T., and Aburatani, H. Differential gene expression profiles of scirrhous gastric cancer cells with high metastatic potential to peritoneum or lymph nodes. Cancer Res., *61:* 889–895, 2001.
21. Ohta, M., Inoue, H., Cotticelli, M. G., Kastury, K., Baffa, R., Palazzo, J., Siprashvili, Z., Mori, M., McCue, P., Druck, T., Croce, C. M., and Huebner, K. The FHIT gene, spanning the chromosome 3p14.2 fragile site and renal carcinoma-associated t(3;8) breakpoint, is abnormal in digestive tract cancers. Cell, *84:* 587–597, 1996.
22. Chang, N. S., Doherty, J., and Ensign, A. JNK1 physically interacts with WW domain-containing oxidoreductase (WOX1) and inhibits WOX1-mediated apoptosis. J. Biol. Chem., *278:* 9195–9202, 2003.

[CANCER RESEARCH 63, 7791–7798, November 15, 2003]

SB-431542 and Gleevec Inhibit Transforming Growth Factor-β-Induced Proliferation of Human Osteosarcoma Cells

Shigeo Matsuyama,[1,2,3] Manabu Iwadate,[2] Miki Kondo,[1,2] Masao Saitoh,[1] Aki Hanyu,[2] Kiyoshi Shimizu,[4] Hiroyuki Aburatani,[5] Hiromu K. Mishima,[3] Takeshi Imamura,[2] Kohei Miyazono,[1,2] and Keiji Miyazawa[1]

[1]Department of Molecular Pathology, Graduate School of Medicine, University of Tokyo, Tokyo; [2]Department of Biochemistry, The Cancer Institute of the Japanese Foundation for Cancer Research, Tokyo; [3]Department of Ophthalmology, Hiroshima University School of Medicine, Hiroshima; [4]Pharmaceutical Research Laboratory, Kirin Brewery Co., Ltd., Gunma; [5]Genome Science Division, Research Center for Advanced Science and Technology, University of Tokyo, Tokyo, Japan

ABSTRACT

Transforming growth factor-β (TGF-β) has growth-stimulating effects on mesenchymal cells and several tumor cell lines. The signaling pathway for this effect is, however, not well understood. We examined how TGF-β stimulates proliferation of MG63 human osteosarcoma cells. Two distinct type I receptors for TGF-β, ALK-1 and ALK-5, were expressed and functional in MG63 cells. Of these two receptors, ALK-5 appears to be responsible for the growth stimulation because expression of constitutively active ALK-5, but not ALK-1, stimulated proliferation of MG63 cells. SB-431542 (0.3 μM), a novel inhibitor of ALK4/5/7 kinase, suppressed TGF-β-induced growth stimulation. DNA microarray analysis as well as quantitative real-time PCR analysis of RNAs from TGF-β-treated cells demonstrated that several growth factors, including platelet-derived growth factor AA, were induced in response to TGF-β in MG63 cells. Gleevec (1 μM) as well as AG1296 (5 μM) inhibited TGF-β-induced growth stimulation of MG63 cells, suggesting that platelet-derived growth factor AA was mainly responsible for the growth-stimulatory effect of TGF-β. We also examined the mechanisms of perturbation of growth-suppressing signaling in MG63 cells. We found that expression of c-Myc, which is down-regulated by TGF-β in many other cells, was up-regulated in MG63 cells, suggesting that up-regulation of c-Myc expression may be the mechanism canceling growth-suppressing signaling of TGF-β in MG63 cells.

INTRODUCTION

TGF[6]-β is a prototype of the cytokines of the TGF-β superfamily, which includes TGF-βs, activins/inhibins, and BMPs (1). Members of the TGF-β superfamily have pleiotropic functions in a wide variety of target cells in physiological as well as pathological processes. One outstanding feature of TGF-β is its growth-inhibitory effect (2, 3). TGF-β acts as a potent growth inhibitor for divergent cell types, including epithelial, endothelial, and hematopoietic cells. Loss of TGF-β-mediated growth inhibition is thought to play a role in tumorigenesis (2). TGF-β also acts as a growth stimulator for some cells of mesenchymal origin such as fibroblasts, chondrocytes, and osteoblasts, as well as several tumor cell lines (4).

The signal transduction pathways leading to the growth inhibition have been studied well at the molecular level (2). TGF-β binds to two different types of serine/threonine kinase receptors, termed type I and type II. Type I receptor is activated by type II receptor upon ligand binding and transduces signals into cytoplasm through phosphorylation of receptor-regulated Smads. ALK-5 is a ubiquitously expressed type I receptor for TGF-β, transmitting signals via Smad2/3. ALK-1 is also a type I receptor for TGF-β; it is predominantly expressed in vascular endothelial cells and transmits signals via Smad1/5 (5). Phosphorylated receptor-regulated Smads interact with Co-Smad (Smad4), translocate to the nucleus, and regulate transcription of target genes in cooperation with transcriptional activators/repressors as well as with coactivators/corepressors (6).

In most types of cells, TGF-β arrests cell cycle progression in the G_1 phase by down-regulating expression of c-Myc and cdc25A and up-regulating that of CDKIs, $p21^{WAF1/CIP1}$ and/or $p15^{Ink4B}$ (2). A Smad-responsive element was identified in the c-myc promoter (7, 8), and the activated Smad complex (Smad2/3-Smad4) has been found to suppress transcription of c-myc in cooperation with p107 and E2F4/5 (8). Down-regulation of c-Myc thus leads to induction of $p21^{WAF1/CIP1}$ and $p15^{Ink4B}$, because c-Myc physically interacts with Smad2/3 and suppresses the function of Sp1-Smad complex in the transcriptional activation of $p21^{WAF1/CIP1}$ and $p15^{Ink4B}$ (9, 10). In contrast, pathways leading to the growth stimulation by TGF-β have not been well elucidated. Thus far, several mechanisms for this growth stimulation have been proposed. TGF-β-induced up-regulation of growth factors including PDGF and FGF has been reported in fibroblasts, Ito cells, and prostate cancer cells (11–18). Down-regulation of CDKIs by TGF-β has been reported in rat osteoblasts ($p57^{Kip2}$; Refs. 19, 20) and H-ras-transfected colon carcinoma cells ($p21^{WAF1/CIP1}$; Refs. 21). Recently, Goumans *et al.* (22) reported that ALK-1 but not ALK-5 acts as a signaling receptor for TGF-β in the transduction of cell proliferation signals in endothelial cells.

Osteosarcoma is one of the most common nonhematological primary malignant tumors of bone (23). Bone is an organ that produces and stores large amounts of TGF-β (24). Recent findings suggest that TGF-β is involved in the progression of osteosarcoma; TGF-β stimulates the growth of several osteosarcoma cell lines in culture (25–27), and overexpression of TGF-β is observed in osteosarcoma tissue by immunohistochemistry, mRNA *in situ* hybridization, and RT-PCR (28, 29). It thus appears important to elucidate how TGF-β acts on osteosarcoma cells.

In the present study, we examined the signal transduction mechanism for the growth-stimulating effect of TGF-β on MG63 human osteosarcoma cells. We found that SB-431542, a novel TGF-β type I kinase inhibitor, as well as Gleevec, inhibited TGF-β-stimulated proliferation of MG63 cells.

MATERIALS AND METHODS

Chemicals, Antibodies, and Recombinant Adenoviruses. SB-431542 was synthesized as described (30) and stored as a solution in DMSO. This solution was used after diluting with medium for each assay. Gleevec (STI571) capsules were purchased from Novartis Pharma (Basel, Switzerland). The contents of one capsule were dissolved in 17 ml of distilled water, centrifuged, filtered, and used as 10 mM stock solution. AG1296 was from Calbiochem (San Diego, CA). TGF-β1, TGF-β3, and BMP-6 were from R & D systems (Minneapolis, MN). Activin-A was a generous gift from Dr. Eto (Ajinomoto Co. Ltd., Tokyo, Japan). FGF-2, HB-EGF, PDGF-AA, and PDGF-BB were

Received 4/4/03; revised 9/3/03; accepted 9/8/03.

The costs of publication of this article were defrayed in part by the payment of page charges. This article must therefore be hereby marked *advertisement* in accordance with 18 U.S.C. Section 1734 solely to indicate this fact.

Requests for reprints: Kohei Miyazono, Department of Molecular Pathology, Graduate School of Medicine, University of Tokyo, 7-3-1 Hongo, Bunkyo-ku, Tokyo 113-0033, Japan. Phone: 81-3-5841-3345; Fax: 81-3-5841-3354; E-mail: miyazono-ind@umin.ac.jp.

S. Matsuyama and M. Iwadate contributed equally to this work.

[6] The abbreviations used are: TGF, transforming growth factor; BMP, bone morphogenetic protein; ALK, activin receptor-like kinase; CDKI, cyclin-dependent kinase inhibitor; PDGF, platelet-derived growth factor; FGF, fibroblast growth factor; RT-PCR, reverse transcription-PCR; HB-EGF, heparin-binding EGF-like growth factor; PAI-1, plasminogen activator inhibitor 1; PlGF, placenta growth factor.

from PeproTech (Rocky Hill, NJ). Anti-phospho-Smad1/5 antibody was from Cell Signaling Technology (Beverly, MA). Anti-phospho-Smad2 antibody was from United Biomedical, Inc. (Hauppauge, NY). Anti-Smad1 antibody and anti-Smad2 antibody were from Transduction Laboratories (Lexington, KY). Anti-c-Myc antibody and anti-p21 antibody were from Oncogene Research Products (San Diego, CA). Anti-lamin A/C antibody was from Santa Cruz Biotechnology (Santa Cruz Biotechnology, Santa Cruz, CA). Anti-α-tubulin antibody (T9026) was from Sigma-Aldrich (St. Louis, MO). Antisera against type I receptors were described previously (31). Recombinant adenoviruses carrying LacZ, a constitutively active form of ALK-1 (ALK-1QD), or ALK-5 (ALK-5TD) were described previously (32, 33).

Cell Culture. MG63 human osteosarcoma cells were maintained in Minimum Essential Medium (Life Technologies, Inc., Carlsbad, CA) containing 10% fetal bovine serum, 1% nonessential amino acids, and 1% penicillin/streptomycin. NIH3T3 cells were maintained in DMEM (Sigma-Aldrich, St. Louis, MO) containing 10% fetal bovine serum, 1% nonessential amino acids, and 1% penicillin/streptomycin.

Cell Proliferation Assay. To explore the effects of ligands, cells were seeded at a density of 8×10^4 cells/well in 6-well plates and starved (0.1% FCS for MG63 cells and 0.5% FCS for NIH3T3 cells) for 24 h before ligand stimulation. Media containing various ligands were exchanged at 48-h intervals. Cells were trypsinized and counted by a Coulter counter on days 2, 4, and 6 after ligand stimulation. The experiments were performed in triplicate. To explore the effects of constitutively active receptors, cells were seeded at a density of 2×10^5 cells/well in 6-well plates. The next day, cells were infected with adenoviruses carrying various cDNAs at a multiplicity of infection of 100. Cells were trypsinized and counted on day 3.

Thymidine Incorporation Assay. Cells were seeded at a density of 2×10^4 cells/well in 24-well plates and cultured overnight. Then serum concentration in the medium was decreased to 0.1%, and the cells were incubated for another 24 h, followed by stimulation with various ligands. Forty-eight h after stimulation, the cells were labeled with [^{3}H]thymidine for 2 h. Thymidine incorporation into the TCA-insoluble fraction was analyzed as described previously (34).

Immunoblotting, Affinity Cross-Linking, and Immunoprecipitation. Immunoblotting was performed as described previously (34). Nuclear extract was prepared using NE-PER Nuclear and Cytoplasmic Extraction kit (Pierce Biotechnology, Rockford, IL). For affinity cross-linking, recombinant TGF-β1 was iodinated using the Chloramine-T method. MG63 cells were affinity-labeled with [^{125}I]-labeled TGF-β1 using 0.27 mM disuccinimidyl suberate (Pierce Biotechnology), followed by immunoprecipitation using specific antisera against ALK-1 or ALK-5. Immune complexes were analyzed as described previously (34).

RNA Extraction and RT-PCR Analysis. Total RNA was extracted from MG63 cells using ISOGEN (Nippon Gene, Toyama, Japan). For RT-PCR analysis, first-strand DNA was synthesized using the Superscript First-Strand Synthesis System (Invitrogen, Carlsbad, CA) with random hexamer primers. Expression of various signaling components was examined by semiquantitative RT-PCR analysis. PCR products were separated by electrophoresis in agarose gels (1%) and visualized with ethidium bromide. The primer sequences, PCR programs, and expected sizes of PCR products were described previously (35).

Oligonucleotide Microarray Analysis. Total RNAs were extracted from MG63 or HaCaT cells at 0, 1, and 4 h after stimulation by TGF-β3 (1 ng/ml). We used the total RNAs to prepare cRNA and conducted oligonucleotide microarray analysis using GeneChip Human Genome U95A (Affymetrix, Santa Clara, CA) according to the manufacturer's instructions.

Quantitative Real-Time PCR Analysis. Total RNAs were extracted from MG63 cells after various treatments, and first-strand cDNAs were synthesized using the Superscript First-Strand Synthesis System (Invitrogen) with random hexamer primers. Quantitative real-time RT-PCR analysis was performed using the GeneAmp 5700 Sequence Detection System (Applied Biosystems, Foster City, CA) as described (33). The primer sequences are available upon request.

RESULTS

TGF-β Stimulates Proliferation of MG63 Cells. MG63 cells were cultured in the presence of 0.1% FBS, and cell numbers were counted at 48-h intervals (Fig. 1*A*). Cell numbers were significantly increased (1.5-fold at day 4) by TGF-β treatment (1 ng/ml), although this effect was rather late in onset and first appeared at day 4. We also examined the effect of TGF-β on DNA synthesis by MG63 cells (Fig. 1*B*). TGF-β caused a dose-dependent increase in [^{3}H]thymidine incorporation. Maximal response was observed above the TGF-β concentration of 100 pg/ml. The response was maintained even at higher concentrations up to 5 ng/ml. These results indicate that TGF-β positively regulates proliferation of MG63 cells.

ALK-1 Is Expressed and Functional in MG63 Cells. To characterize the signaling pathways of the TGF-β superfamily in MG63 cells, we first examined the expression profiles of signaling components of TGF-β superfamily, *i.e.*, the receptors and Smad proteins, by RT-PCR analysis. Most of the signaling components except for ALK-6, ActR-IIB, and Smad6 were detected in MG63 cells (data not shown). Smad6 was not detected without TGF-β stimulation but was detected after stimulation with TGF-β. Notably, ALK-1 was expressed in MG63 cells. ALK-1 is a type I receptor for TGF-β predominantly expressed in vascular endothelial cells. In vascular endothelial cells, ALK-1 is reported to be involved in TGF-β-induced cell growth and cell motility (22). Because it appeared possible that the growth-stimulatory effect of TGF-β on MG63 cells could be attributed to the presence of ALK-1, we examined whether ALK-1 is functional in MG63 cells.

MG63 cells were affinity-labeled with [^{125}I]-labeled TGF-β followed by cross-linking and immunoprecipitation by antisera against ALK-1 or ALK-5 (Fig. 2*A*). Cross-linked bands were observed when anti-ALK-1 or anti-ALK-5 was used but not when preimmune serum was used. This result indicated that ALK-1 as well as ALK-5 is expressed on the MG63 cell surface and functional in binding to TGF-β.

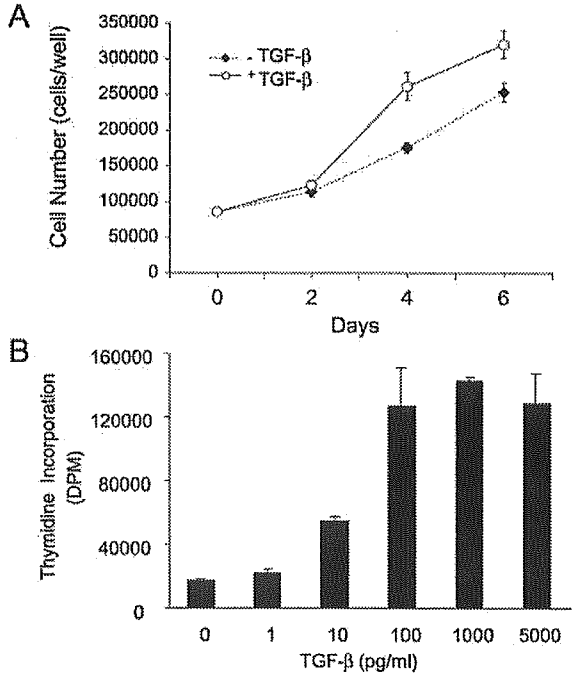

Fig. 1. TGF-β positively regulates proliferation of MG63 cells. *A*, cell proliferation assay. MG63 cells were cultured in the presence or absence of TGF-β3 (1 ng/ml), and cell numbers were counted on days 2, 4, and 6 after treatment. Each value represents the mean of triplicate determinations; *bars*, SD. *B*, [^{3}H]thymidine incorporation assay. MG63 cells were treated with various concentrations of TGF-β3 (0–5 ng/ml) and labeled with [^{3}H]thymidine for 2 h. Each value represents the mean of triplicate determinations; *bars*, SD.

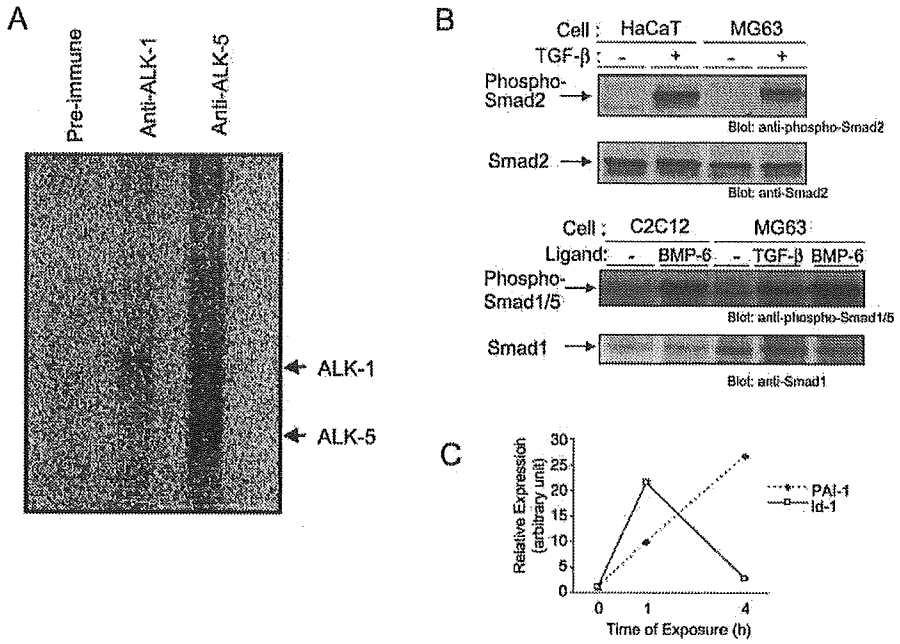

Fig. 2. ALK-1 is expressed and functional in MG63 cells. *A*, affinity cross-linking and immunoprecipitation analysis. MG63 cells were affinity-labeled with [^{125}I]-labeled TGF-β1, followed by immunoprecipitation using specific antisera against ALK-1 or ALK-5. *B*, immunoblotting analysis of phosphorylated Smads. MG63 cells were starved for 24 h and treated with TGF-β3 (1 ng/ml) for 1 h (for Smad2 phosphorylation) or 2 h (for Smad1/5 phosphorylation). Total cell lysates were separated by SDS-PAGE and transferred to polyvinylidene difluoride membranes, which were blotted with anti-phospho-Smad2 antibody and anti-Smad2 antibody (*upper panel*) or anti-phospho-Smad1/5 antibody and anti-Smad1 antibody (*lower panel*). Positive controls were as follows: HaCaT cells treated with TGF-β3 (1 ng/ml) for 1 h (for Smad2), and C2C12 cells treated with BMP-6 (50 ng/ml) for 1 h (for Smad1/5). *C*, relative mRNA expression of target genes for ALK-5 (PAI-1) and ALK-1 signal (Id-1) was measured by quantitative real-time PCR. Total RNAs were extracted from MG63 cells before and after TGF-β treatment. Fold-induction by TGF-β treatment is indicated. Each value represents the mean of triplicate determinations; *bars*, SD.

We next examined whether ALK-1 in MG63 cells can transmit signals. It has been reported that TGF-β stimulation of endothelial cells induces phosphorylation of Smad1/5 as well as Smad2/3; the former is ALK-1-dependent, and the latter is ALK-5-dependent (22). We observed phosphorylation of Smad1/5 as well as Smad2/3 in MG63 cells in response to TGF-β stimulation (Fig. 2*B*). We also quantified the expression level of mRNA for PAI-1 (as an ALK-5 target) as well as Id1 (as an ALK-1 target; Ref. 22; also Fig. 4*A*) by quantitative real-time PCR analysis (Fig. 2*C*). In response to TGF-β, expression of PAI-1 as well as Id1 was induced, suggesting that both ALK-5 and ALK-1 signals were transmitted in MG63 cells.

SB-431542 Inhibited Cell Proliferation Induced by TGF-β. The next question we addressed was which of the type I receptors is responsible for the growth stimulation of MG63 cells. We used SB-431542, which is reported to be a specific inhibitor of ALK-4, ALK-5, and ALK-7, the type I receptors for activin, TGF-β, and nodal (36). Cell proliferation assay was performed in the presence of 0.3 μM SB-431542. As shown in Fig. 3*A*, SB-431542 inhibited cell proliferation induced by TGF-β. In contrast, it did not inhibit PDGF-BB-induced cell proliferation, thus excluding the possibility of a nonspecific effect.

The specificity of inhibition of type I receptors was examined by Smad phosphorylation and quantitative real-time PCR analysis. Unexpectedly, SB-431542 inhibited the phosphorylation of both Smad2/3 and Smad1/5 induced by TGF-β (Fig. 3*B*), although it did not inhibit the phosphorylation of Smad1/5 induced by BMP-6. Furthermore, SB-431542 inhibited TGF-β-induced Id-1 expression as well as PAI-1 (data not shown). These results indicated that SB-431542 affected both ALK-1- and ALK-5-mediated signaling induced

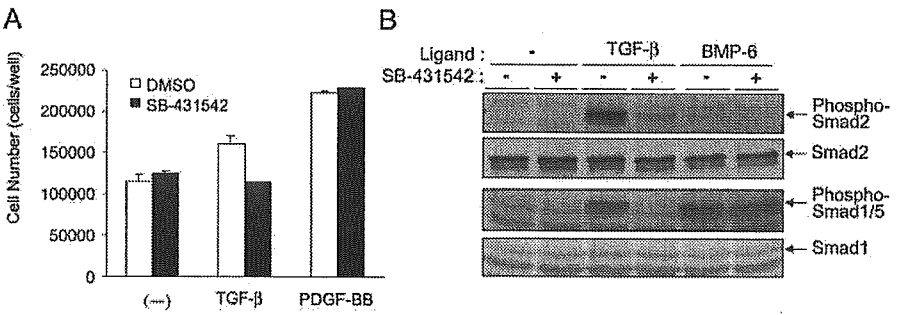

Fig. 3. Effect of SB-431542 on TGF-β-stimulated responses in MG63 cells. *A*, effect of SB-431542 on TGF-β-stimulated cell proliferation. MG63 cells were treated with TGF-β3 (1 ng/ml) or PDGF-BB (10 ng/ml), and cell numbers were counted on day 4. SB-431542 (0.3 μM) or DMSO (vehicle) was added 30 min before ligand stimulation. Each value represents the mean of triplicate determinations; *bars*, SD. *B*, effect of SB-431542 on Smad phosphorylation. MG63 cells were treated with TGF-β3 (1 ng/ml) or BMP-6 (50 ng/ml) for 1 h in the presence or absence of SB-431542 (0.3 μM), which was added 30 min before ligand stimulation. Phosphorylation of Smad proteins was examined by immunoblotting using anti-phospho-Smad2 and anti-Smad2 (*upper two panels*) or anti-phosho-Smad1/5 antibody and anti-Smad1 (*lower two panels*).

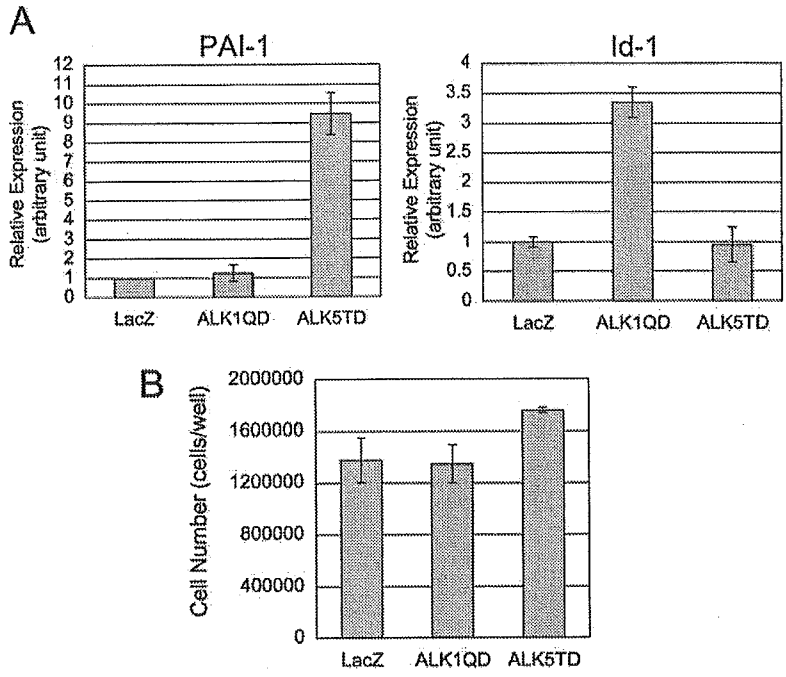

Fig. 4. Effects of constitutively active forms of ALK-1 (ALK-1QD) and ALK-5 (ALK-5TD) on MG63 cells. MG63 cells infected with recombinant adenoviruses carrying LacZ, ALK-1QD, or ALK-5TD at a multiplicity of infection of 100 plaque-forming units/cell were harvested 72 h after infection. *A*, induction of target genes for ALK-5 (PAI-1) and ALK-1 (Id-1) was examined by quantitative real-time PCR analysis. *B*, cell numbers were counted. Each value represents the mean of triplicate determinations; *bars*, SD.

by TGF-β ligand. The type I receptor responsible for growth stimulation could not be identified with the use of SB-431542.

Constitutively Active ALK-5 but not ALK-1 Induced Proliferation of MG63 Cells. We next examined effects of constitutively active forms of ALK-1 (ALK-1QD) and ALK-5 (ALK-5TD) on proliferation of MG63 cells. MG63 cells were infected with adenoviruses carrying LacZ, ALK-1QD, or ALK-5TD. Expression of ALK-1QD caused induction of Id-1, whereas expression of ALK-5TD caused induction of PAI-1 (Fig. 4*A*), indicating that both receptors transmitted signals in MG63 cells. Results of cell proliferation assay, however, demonstrated that ALK-5 but not ALK-1 induced cell proliferation in MG63 cells (Fig. 4*B*). We thus concluded that ALK-5 is mainly responsible for growth stimulation by TGF-β in MG63 cells.

Activin-A but not BMP-6 Stimulated Proliferation of MG63 Cells. We also examined the effects of other ligands in the TGF-β superfamily, *i.e.*, activin-A and BMP-6, on proliferation of MG63 cells. In most cell types, activin-A transmits signals via ALK-4 and Smad2/3, whereas BMP-6 transmits Smad1/5 signals. The selectivity of signal transduction in MG63 cells was confirmed on the basis of induction of target genes. Activin-A induced PAI-1, although the intensity of induction was weaker than that by TGF-β, whereas it did not induce Id1. In contrast, BMP-6 induced Id1, but induced PAI-1 only weakly (Fig. 5*A*).

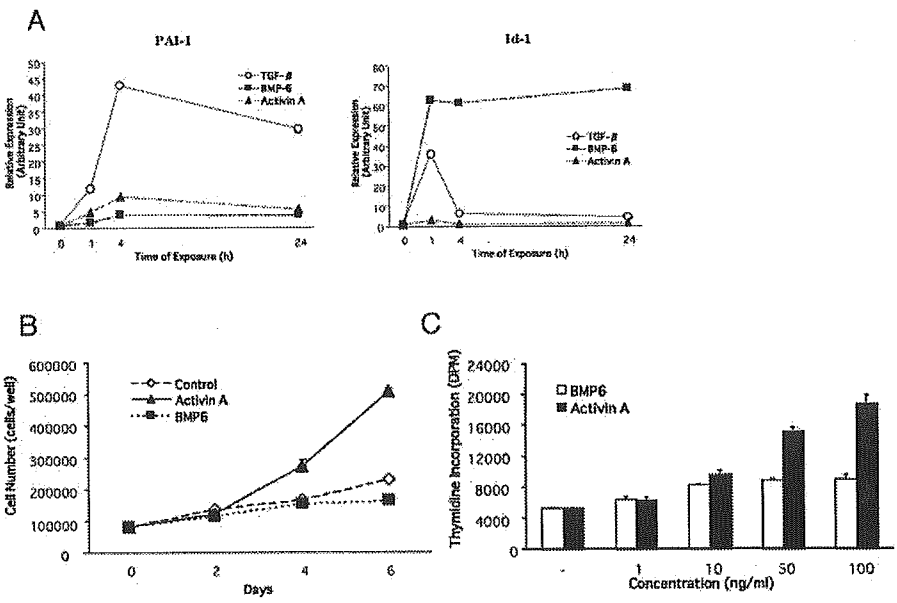

Fig. 5. Effects of activin-A and BMP-6 on MG63 cells. *A*, induction of target genes (PAI-1 and Id-1) was examined in cells treated with TGF-β3 (1 ng/ml), BMP-6 (50 ng/ml), or activin-A (100 ng/ml) for 0, 1, 4, or 24 h by quantitative real-time PCR. Each value represents the mean of triplicate determinations; *bars*, SD. *B*, cell proliferation assay was performed in cells treated with activin-A (100 ng/ml) or BMP-6 (50 ng/ml). Cells were counted on days 2, 4, and 6. Each value represents the mean of triplicate determinations; *bars*, SD. *C*, [^{3}H]thymidine incorporation assay was performed in the presence of various concentrations of activin-A or BMP-6 (0–100 ng/ml). Each value represents the mean of triplicate determinations; *bars*, SD.

Table 1 *Genes regulated by TGF-β in MG63 cells and HaCaT cells*

Total RNAs were extracted from MG63 or HaCaT cells at 0, 1, and 4 hours after stimulation by TGF-β3 (1 ng/ml) and used to prepare cRNA. Oligonucleotide microarray analysis was conducted using GeneChip Human Genome U95A (Affymetrix). Intensity <50 means that the level of expression is as low as background.

		MG63					HaCaT				
		Control	TGF-β 1 h		TGF-β 4 h		Control	TGF-β 1 h		TGF-β 4 h	
Accession number	Description	Intensity	Intensity	Fold change	Intensity	Fold change	Intensity	Intensity	Fold change	Intensity	Fold change
Representative TGF-β target genes											
M14083	*PAI-1*	105.2	1021.1	9.4	3173.3	29.7	50.7	259.3	5.1	695.9	12.9
X51345	*jun B*	388.5	1429.9	3.7	466.9	1.6	291.1	596.6	2.8	474.9	2.1
AF010193	*Smad7*	88.1	412.2	4.7	228.6	2.6	46.4	173.3	4.7	117.9	3.2
U76702	*follistatin-like 3*	8.4	59.8	7.1	385.3	35.8	80.9	121.2	1.5	482.7	4.7
U03106	*p21*	133	341.8	2.8	239.4	1.1	252.7	470.5	1.9	470.5	2.6
V00568	*c-Myc*	166	500.8	3	263.4	1.6	295.3	198.1	−1.5	137.4	−2.1
Representative BMP target genes											
X77956	*Id-1*	106.3	2291.3	21.6	295.6	2.8	1740.9	2477.6	1.4	914.4	−1.9
D13891	*Id-2*	78.2	555.1	7.1	125.6	1.6	37.8	101.2	2.8	25.6	−1.7
AL021154	*Id-3*	171.8	1037.1	6	544.1	3.2	748.1	963.5	1.3	879.6	1.2
AF035528	*Smad6*	53	100.9	1.9	119.1	2.2	6.2	17.6	1.4	20.4	>2.2
Growth factors and receptors											
X06374	*PDGF-A*	46.7	46.7	2.3	240.6	7.5	127.3	100.5	−1.3	146	1.1
X63966	*PDGF-B*	−59.3	−56.6	>1.5	−34.8	<−1.9	−10.9	−14.7	<−1.7	−20	<−2.3
M21574	*PDGFRα*	398.4	375.4	−1.1	228.2	−2	9.1	9.9	1.1	8	−1.1
J03278	*PDGFRβ*	231.6	243.6	1.1	553.3	2.5	40.4	16.1	−1.9	23.4	−1.2
M27968	*FGF-2*	99.3	105	1.1	327.1	3.6	13.5	13.5	1.3	17.4	1.3
X54936	*PIGF*	−3.6	8.7	>3.1	117.1	>18.3	11	6.1	−1.8	−1.4	<−2.8
M60278	*HBEGF*	0.9	158.7	>26.7	260	>34.4	−12.1	31.5	>9.4	0.6	>2.8

Effects of these ligands on proliferation of MG63 cells were then examined. Activin-A stimulated proliferation and thymidine incorporation in MG63 cells at concentrations around 50–100 ng/ml, whereas BMP-6 was only weakly effective (Fig. 5, *B* and *C*). These findings further confirmed that the Smad2/3 pathway but not the Smad1/5 pathway plays a major role in transmitting proliferation signals in MG63 cells.

DNA Microarray Analysis of TGF-β-regulated Genes in MG63 Cells. To elucidate the signaling pathway involved in the cell proliferation induced by TGF-β, we analyzed TGF-β-regulated genes using DNA microarray. We used HaCaT cells as a reference, because their growth is inhibited by TGF-β. Several representative target genes of TGF-β signaling were induced in MG63 cells (Table 1), indicating that the signaling pathway of TGF-β was not greatly altered in the cells. However, we found four unique features:

(*a*) Several growth factors were induced in MG63 cells in response to TGF-β stimulation. They were PDGF-A, FGF-2, HB-EGF, and PlGF. In HaCaT cells, significant induction of these growth factors was not observed. It is thus possible that growth stimulation of MG63 cells by TGF-β is mediated through the induction of these growth factors.

(*b*) Expression of c-Myc was up-regulated in MG63 cells. In most cells including HaCaT cells, expression of c-Myc is down-regulated after TGF-β stimulation.

(*c*) Expression of $p21^{WAF1/CIP1}$ was up-regulated in both MG63 cells and HaCaT cells, only transiently in MG63 cells but in rather sustained fashion in HaCaT cells.

(*d*) As expected from the observation that MG63 cells express ALK-1, Id proteins were rapidly induced in MG63 cells. As shown in Fig. 4, the possibility of involvement of ALK-1 in the growth-stimulating signaling had already been excluded. We thus further examined the first three features.

TGF-β-induced Growth Factors in MG63 Cells: Their Effects on Proliferation of MG63 Cells. Induction of PDGF-A, FGF-2, HB-EGF, and PlGF by TGF-β was confirmed by real-time PCR analysis (Fig. 6 and data not shown). These results are consistent with those of DNA microarray analysis. We also observed that induction of these growth factors was completely inhibited by SB-431542 (data not shown). Among the induced growth factors, however, PlGF seemed unlikely to be involved in the growth stimulation of MG63 cells, because the receptor for PlGF (Flt1) is not expressed in the cells.

We next examined effects of growth factors that were up-regulated by TGF-β in MG63 cells. As shown in Fig. 7*A*, PDGF-AA and FGF-2 were effective in stimulating thymidine incorporation in MG63 cells, whereas HB-EGF was only weakly effective.

To determine which of the three growth factors, PDGF-AA, FGF-2, and HB-EGF, is mainly involved in the growth stimulation by TGF-β, we used a tyrosine kinase inhibitor, Gleevec (STI571), which inhibits PDGF receptor kinase (Ref. 37; Fig. 7*B*). MG63 cells were cultured in the presence of the inhibitor and treated with TGF-β, PDGF-AA, FGF-2, or HB-EGF. Gleevec (1 μM) inhibited the growth stimulation induced by TGF-β as well as that by PDGF-AA but did not inhibit the stimulatory effects of FGF-2 and HB-EGF. A similar result was obtained when AG1296, another inhibitor of the PDGF receptor

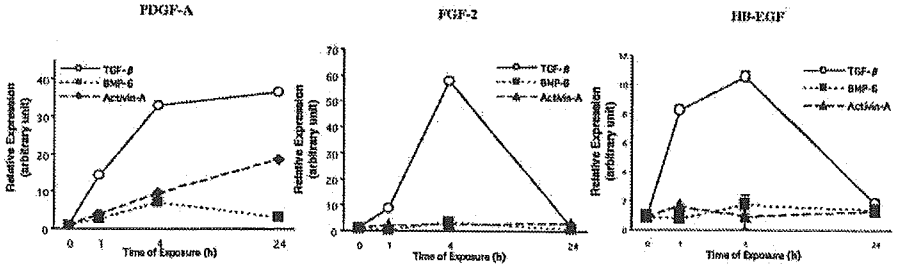

Fig. 6. Up-regulation of growth factors by signaling from the TGF-β superfamily. MG63 cells were starved for 24 h and treated with TGF-β3 (1 ng/ml), BMP-6 (50 ng/ml), or activin-A (100 ng/ml). Total RNAs were extracted from the cells at 0, 1, 4, and 24 h after treatment and analyzed by quantitative real-time PCR using specific primers for PDGF-A, FGF-2, or HB-EGF. Each value represents the mean of triplicate determinations; *bars*, SD.

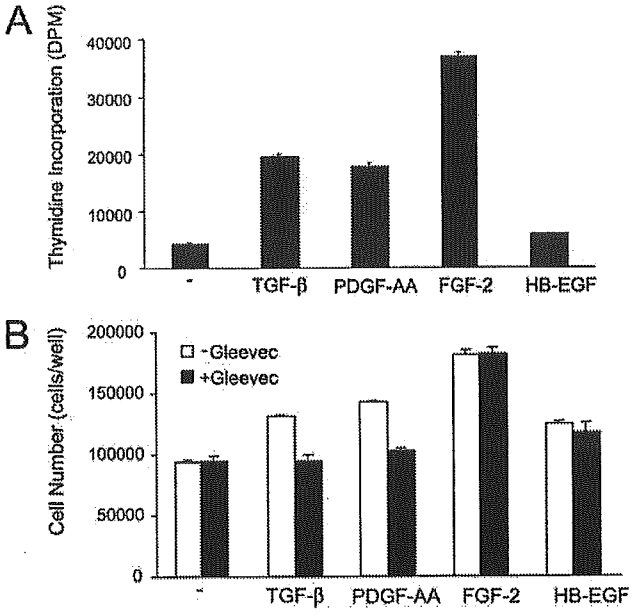

Fig. 7. Effect of up-regulated growth factors on proliferation of MG63 cells. *A*, [^{3}H]thymidine incorporation assay was performed in the presence of TGF-β3 (1 ng/ml), PDGF-AA (10 ng/ml), FGF-2 (5 ng/ml), or HB-EGF (5 ng/ml). Each value represents the mean of triplicate determinations; *bars*, SD. *B*, cell proliferation assay was performed in the presence of various ligands (concentration of each ligand is described above). The effect of Gleevec (1 μM) was also examined. Gleevec was added 30 min before ligand stimulation. Cells were counted on day 4. Each value represents the mean of triplicate determinations; *bars*, SD.

kinase (38), was used (5 μM; data not shown). These results suggested that the effect of TGF-β was mediated principally through PDGF signaling, although the involvement of FGF signaling cannot be excluded.

We also examined the induction of growth factors by activin-A and BMP-6 (Fig. 6). Activin-A, which stimulated growth of MG63 cells, induced PDGF-A but neither FGF-2 nor HB-EGF. BMP-6, which did not stimulate the growth of MG63 cells, induced none of the three growth factors. These results further supported a major role of PDGF signaling in the growth stimulation of MG63 cells by ligands of the TGF-β superfamily.

Control of Cell Cycle Regulators by TGF-β in MG63 Cells. It is also important to elucidate why growth-inhibitory signaling by TGF-β is ineffective in MG63 cells. As described above, expression of both c-Myc and p21$^{WAF1/CIP1}$ was up-regulated on DNA microarray analysis. We confirmed the induction of c-Myc and p21$^{WAF1/CIP1}$ using quantitative real-time PCR analysis and found that it was inhibited by SB-431542 (data not shown). p15 mRNA was not detected in MG63 cells.

We further examined the protein levels of c-Myc and p21$^{WAF1/CIP1}$ after TGF-β treatment (Fig. 8*A*). Expression of c-Myc protein was up-regulated from 12 h after TGF-β treatment, and this up-regulation was maintained even at 24 h after the treatment. Expression of p21$^{WAF1/CIP1}$ protein was also up-regulated, but maximal expression was observed at 12 h, with decrease to basal level by 24 h. We also confirmed that nuclear p21$^{WAF1/CIP1}$, which has cell cycle inhibitory activity, was actually up-regulated by cell-fractionation experiment (Fig. 8*B*). These results suggest that, among the growth-inhibitory signals by TGF- β, the pathway leading to c-Myc down-regulation was abrogated, and that a signal up-regulating c-Myc expression may be transmitted in MG63 cells.

Effects of SB-431542 and Gleevec on TGF-β-induced Proliferation of NIH3T3 Cells. Finally, we examined the effects of SB-431542 and Gleevec on TGF-β-induced proliferation of cell lines other than MG63. Among several cell lines tested, NIH3T3 cells exhibited TGF-β-induced growth stimulation, which is comparable to that of MG63 cells. The growth stimulation was inhibited by SB-431542 but not by Gleevec (Fig. 9). These results suggested that TGF-β-induced growth stimulation is mediated through various mechanisms, which appear to depend on cell types.

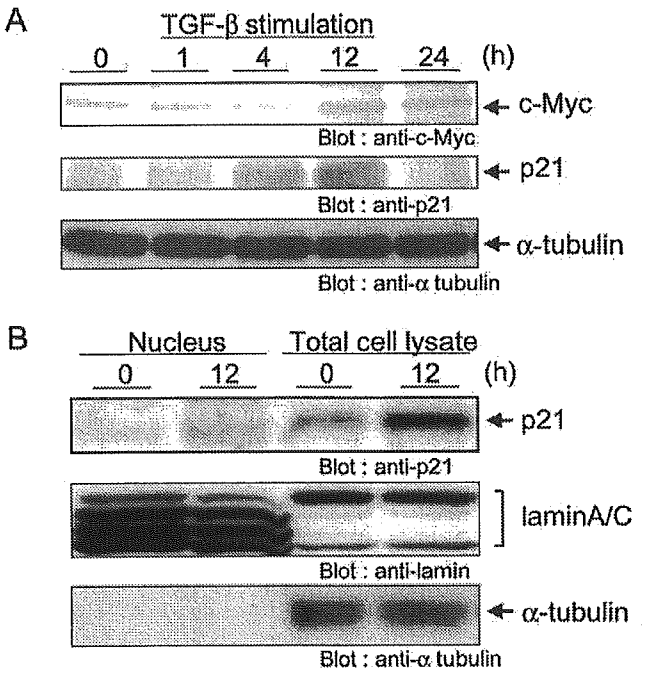

Fig. 8. Up-regulation of c-Myc and p21$^{WAF1/CIP1}$ by TGF-β in MG63 cells. *A*, MG63 cells were starved for 24 h and then treated with TGF-β3 (1 ng/ml). At various times after treatment (0, 1, 4, 12, and 24 h), cell lysates were prepared. Protein levels of c-Myc (*upper panel*) and p21$^{WAF1/CIP1}$ (*middle panel*) and α-tubulin (*bottom panel*) were examined by immunoblotting of the total lysates with anti-c-Myc, anti-p21, or anti-α-tubulin antibody, respectively. *B*, total cell lysates and nuclear extracts were prepared from MG63 cells at 0 and 12 h after TGF-β treatment (1 ng/ml). Lamin A/C and α-tubulin were used to confirm equal loading of samples as well as the integrity of fractionation.

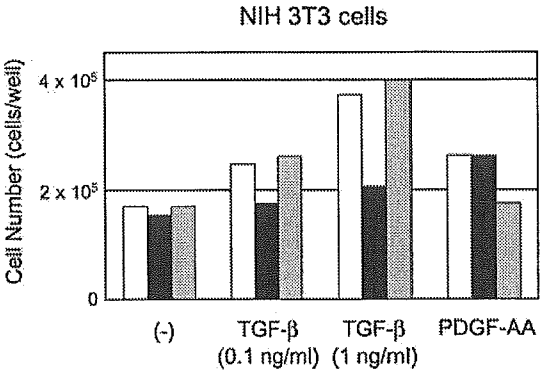

Fig. 9. Effects of SB-431542 and Gleevec on TGF-β-induced proliferation of NIH3T3 cells. NIH3T3 cells were treated with TGF-β (0.1 and 1 ng/ml) or PDGF-AA (10 ng/ml), and cell numbers were counted on day 2 after ligand stimulation. Inhibitors were added 30 min before ligand stimulation. □, control samples; ■, SB-431542 (0.3 μM)-treated samples; ▨, Gleevec (1 μM)-treated samples.

DISCUSSION

In the present study, we examined the pathway of signal transduction by TGF-β leading to proliferation of MG63 osteosarcoma cells. Although the effects of TGF-β on proliferation of MG63 cells are controversial (39–42), we observed significant stimulation of proliferation after TGF-β treatment in the presence of 0.1% FBS, based on an increase in cell number as well as of thymidine incorporation. We found that growth-stimulatory signal was transmitted via the ALK-5 pathway, and that PDGF-A is induced by TGF-β. We also demonstrated that SB-431542, a novel ALK-5 kinase inhibitor, as well as Gleevec (STI571), an inhibitor of PDGF receptor kinase, inhibited the growth stimulation by TGF-β.

Interestingly, ALK-1, a TGF-β type I receptor preferentially expressed in endothelial cells, was found to be expressed on the MG63 cell surface and to bind TGF-β. We further confirmed that ALK-1 was functionally active based on the phosphorylation of Smad1/5 as well as gene expression profiles of targets of the Smad1/5 pathway. The up-regulated genes include those for Id proteins (Id1, Id2, and Id3). Id proteins were originally identified as "inhibitor of differentiation," and their positive roles in cell cycle progression have been reported recently (43). Id proteins negatively regulate CDK inhibitors. In addition, Id2 physically interacts with hypophosphorylated pRb and antagonizes its antiproliferative effect. It thus seemed possible that induction of Id by the ALK-1 pathway is involved in the growth-stimulating effect of TGF-β in MG63 cells. In the present study, however, we observed that ALK-1 signaling is not sufficient for the growth stimulation of MG63 cells. The function of ALK-5 is sufficient and indispensable for the growth stimulation, although the possibility cannot be excluded that ALK1 cooperates with ALK5 and is involved in the growth stimulation.

Analyses of the TGF-β-regulated genes in MG63 cells revealed up-regulation of four growth factors; among them, only PDGF-AA and FGF-2 were effective in stimulating proliferation of MG63 cells when exogenously added. Using specific inhibitors of PDGF receptor kinases, Gleevec and AG1296, we found that PDGF-AA mainly contributed to the growth-promoting action of TGF-β in MG63 cells. This may be because expression of FGF-2 was only transiently up-regulated, whereas that of PDGF-AA was up-regulated in a sustained fashion.

We further examined the expression of cell cycle regulators. Miyazaki *et al.* (44) reported that TGF-β stimulates or down-regulates cell growth through down- or up-regulation of $p21^{WAF1/CIP1}$. $p21^{WAF1/CIP1}$ is one of the direct targets of Smad proteins (10, 45). In MG63 cells, $p21^{WAF1/CIP1}$ was up-regulated by TGF-β, but cell proliferation was still stimulated. This result suggested that certain signaling pathways of TGF-β leading to growth inhibition are still active, but that some mechanism canceling the growth inhibition by $p21^{WAF1/CIP1}$ may become predominant. In this respect, it should be noted that the induction of $p21^{WAF1/CIP1}$ by TGF-β in MG63 cells was only transient. We also observed that c-Myc was up-regulated in a sustained fashion in response to TGF-β stimulation in MG63 cells. Induction of c-Myc by TGF-β has already been reported by Leof *et al.* (11) in AKR-2B cells, which are also growth stimulated by TGF-β. One of the functions of c-Myc in cell cycle progression is to down-regulate expression of CDKIs including $p21^{WAF1/CIP1}$. Thus, up-regulation of c-Myc in MG63 cells may cause the transient induction of $p21^{WAF1/CIP1}$, which may lead, at least in part, to abrogation of growth-inhibitory signaling by TGF-β.

In the present study, we used SB-431542 to selectively inhibit ALK-5 signaling but observed an inhibitory effect of SB-431542 on ligand-induced ALK-1 signaling in MG63 cells. Inman *et al.* (36) reported that this inhibitor was not effective on the constitutively active form of ALK-1 in which Gln-201 was mutated to Asp (QD mutant). There appears to be two possible explanations for this observation. One is that SB-431542 has differential effects on ligand-activated ALK-1 kinase and mutationally activated ALK-1 kinase. Alternatively, ALK-1 requires ALK-5 kinase activity for its activation by ligands. The mechanism of inhibition of ALK-1 signaling by SB-431542 remains to be elucidated.

Many tumor cells are not responsive to TGF-β and sometimes secrete TGF-β. TGF-β may induce growth factor secretion from stromal cells, and the secreted growth factors may in turn enhance proliferation of cancer cells. This is thought to be one mechanism by which TGF-β activity enhances malignancy of cancer (46). Thus, inhibition of growth factor induction may lead to suppression of tumor growth. Moreover, PDGF was reported to cause high interstitial fluid pressure in tumor tissues. High interstitial fluid pressure acts as a barrier to tumor transvascular transport, decreasing uptake of antitumor reagents by tumors. Recently, Pietras *et al.* (47) reported that inhibition of PDGF activity by Gleevec enhanced the efficacy of chemotherapeutic treatment by decreasing the tumor interstitial fluid pressure. In the present study, we found that SB-431542, a novel ALK-4/5/7 inhibitor, can block induction of growth factors including PDGF. Thus, synthetic kinase inhibitors of ALK-5 may have additional effects *in vivo*, mediated through inhibition of PDGF induction, if used together with chemotherapeutic drugs. Development of clinically available ALK-5 kinase inhibitors is thus highly desired.

ACKNOWLEDGMENTS

We thank Hiroko Meguro for technical assistance and Hisako Hirano for secretarial assistance.

REFERENCES

1. Miyazono, K., Kusanagi, K., and Inoue, H. Divergence and convergence of TGF-β/BMP signaling. J. Cell. Physiol., *187:* 265–276, 2001.
2. Massagué, J., Blain, S. W., and Lo, R. S. TGFβ signaling in growth control, cancer, and heritable disorders. Cell, *103:* 295–309, 2000.
3. ten Dijke, P., Goumans, M-J., Itoh, F., and Itoh, S. Regulation of cell proliferation by Smad proteins. J. Cell. Physiol., *191:* 1–16, 2002.
4. Moses, H. L., Yang, E. Y., and Pietenpol, J. A. TGF-β stimulation and inhibition of cell proliferation: new mechanistic insights. Cell, *63:* 245–247, 1990.
5. Oh, S. P., Seki, T., Goss, K. A., Imamura, T., Yi, Y., Donahoe, P. K., Li, L., Miyazono, K., ten Dijke, P., Kim, S., and Li, E. Activin receptor like kinase-1 modulates transforming growth factor-β1 signaling in the regulation of angiogenesis. Proc. Natl. Acad. Sci. USA, *97:* 2626–2631, 2000.
6. Miyazono, K., ten Dijke, P., and Heldin, C-H. TGF-β signaling by Smad proteins. Adv. Immunol., *75:* 115–157, 2000.
7. Yagi, K., Furuhashi, M., Aoki, H., Goto, D., Kuwano, H., Sugamura, K., Miyazono, K., and, Kato, M. c-myc is a downstream target of the Smad pathway. J. Biol. Chem., *277:* 854–861, 2002.
8. Chen, C-R., Kang, Y., Siegel, P. M., and Massagué, J. E2F4/5 and p107 as Smad cofactors linking the TGFβ receptor to *c-myc* repression. Cell, *110:* 19–32, 2002.
9. Feng, X-H., Liang, Y-Y., Liang, M., Zhai, W., and Lin, X. Direct interaction of c-Myc with Smad2 and Smad3 to inhibit TGF-β-mediated induction of the CDK inhibitor $p15^{Ink4B}$. Mol. Cell, *9:* 135–143, 2002.
10. Pardali, K., Kurisaki, A., Morén, A., ten Dijke, P., Kardassis, D., and Moustakas, A. Role of Smad proteins and transcription factor Sp1 in $p21^{WAF1/CIP1}$ regulation by transforming growth factor-β. J. Biol. Chem., *275:* 29224–29256, 2000.
11. Leof, E. B., Proper, J. A., Goustin, A. S., Shipley, G. D., DiCorleto, P. E., and Moses, H. L. Induction of c-sis mRNA and activity similar to platelet-derived growth factor by transforming growth factor β: a proposed model for indirect mitogenesis involving autocrine activity. Proc. Natl. Acad. Sci. USA, *83:* 2453–2457, 1986.
12. Battegay, E. J., Raines, E. W., Seifert, R. A., Bowen-Pope, D. F., and Ross, R. TGF-β induces bimodal proliferation of connective tissue cells via complex control of an autocrine PDGF loop. Cell, *63:* 515–524, 1990.
13. Win, K. M., Charlotte, F., Mallat, A., Cherqui, D., Martin, N., Mavier, P., Preaux, A. M., Dhumeaux, D., and Rosenbaum, J. Mitogenic effect of transforming growth factor- β1 on human Ito cells in culture: evidence for mediation by endogenous platelet-derived growth factor. Hepatology, *18:* 137–145, 1993.
14. Seifert, R. A., Coats, S. A., Raines, E. W., Ross, R., and Bowen-Pope, D. F. Platelet-derived growth factor (PDGF) receptor α-subunit mutant and reconstituted cell lines demonstrate that transforming growth factor-β can be mitogenic through PDGF A-chain-dependent and -independent pathways. J. Biol. Chem., *269:* 13951–13955, 1994.

15. Sintich, S. M., Lamm, M. L. G., Sensibar, J. A., and Lee, C. Transforming growth factor-β1-induced proliferation of the prostate cancer cell line, TSU-Pr1: the role of platelet-derived growth factor. Endocrinology, *140:* 3411–3415, 1999.
16. Kay, E. P., Lee, H. K., Park, K. S., and Lee, S. C. Indirect mitogenic effect of transforming growth factor-β on cell proliferation of subconjunctival fibroblasts. Invest. Ophthalmol. Vis. Sci., *39:* 481–486, 1998.
17. Kay, E. P., Lee, M. S., Seong, G. J., and Lee, Y. G. TGF-βs stimulate cell proliferation via an autocrine production of FGF-2 in corneal stromal fibroblasts. Curr. Eye Res., *17:* 286–293, 1998.
18. Strutz, F., Zeisberg, M., Renziehausen, A., Raschke, B., Becker, V., van Kooten, C., and Müller, G. A. TGF-β1 induces proliferation in human renal fibroblasts via induction of basic fibroblast growth factor (FGF-2). Kidney Int., *59:* 579–592, 2001.
19. Urano, T., Yashiroda, H., Muraoka, M., Tanaka, K., Hosoi, T., Inoue, S., Ouchi, Y., Tanaka, K., and Toyoshima, H. $p57^{Kip2}$ is degraded through the proteasome in osteoblasts stimulated to proliferation by transforming growth factor β1. J. Biol. Chem., *274:* 12197–12200, 1999.
20. Nishimori, S., Tanaka, Y., Chiba, T., Fujii, M., Imamura, T., Miyazono, K., Ogasawara, T., Kawaguchi, H. Igarashi, T., Fujita, T., Tanaka, K., and Toyoshima, H. Smad-mediated transcription is required for transforming growth factor-β1-induced $p57^{Kip2}$ proteolysis in osteoblastic cells. J. Biol. Chem., *276:* 10700–10705, 2001.
21. Yan, Z., Kim, G-Y., Deng, X., and Friedman, E. Transforming growth factor β1 induces proliferation in colon carcinoma cells by Ras-dependent, smad-independent down-regulation of p21cip1. J. Biol. Chem., *277:* 9870–9879, 2002.
22. Goumans, M-J., Valdimarsdottir, G., Itoh, S., Rosendahl, A., Sideras, P., and ten Dijke, P. Balancing the activation state of the endothelium via two distinct TGF-β type I receptors. EMBO J., *21:* 1743–1753, 2002.
23. Ragland, B. D., Bell, W. C., Lopez, R. R., and Siegal, G. P. Cytogenetics and molecular biology of osteosarcoma. Lab. Invest., *82:* 365–373, 2002.
24. Seyedin, S. M., Thompson, A. Y., Bentz, H., Rosen, D. M., McPherson, J. M., Conti, A., Siegel, N. R., Galluppi, G. R., and Piez, K. A. Cartilage-inducing factor-A: apparent identity to transforming growth factor-β. J. Biol. Chem., *261:* 5693–5695, 1986.
25. Pfeilschifter, J., D'Souza, S. M., and Mundy, G. R. Effects of transforming growth factor-β on osteoblastic osteosarcoma cells. Endocrinology, *121:* 212–218, 1987.
26. Kloen, P., Jennings, C. L., Gebhardt, M. C., Springfield, D. S., and Mankin, H. J. Expression of transforming growth factor-β (TGF-β) receptors, TGF-β1 and TGF-β2 production and autocrine growth control in osteosarcoma cells. Int. J. Cancer, *58:* 440–445, 1994.
27. Reed, B. Y., Zerwekh, J. E., Antich, P. P., and Pak, C. Y. Fluoride-stimulated [^{3}H]thymidine uptake in a human osteoblastic osteosarcoma cell line is dependent on transforming growth factor β. J. Bone Miner. Res., *8:* 19–25, 1993.
28. Franchi, A., Arganini, L., Baroni, G., Calzolari, A., Capanna, R., Campanacci, D., Caldora, P., Masi, L., Brandi, M. L., and Zampi, G. Expression of transforming growth factor β isoforms in osteosarcoma variants: association of TGF β1 with high-grade osteosarcomas. J. Pathol., *185:* 284–289, 1998.
29. Kloen, P., Gebhardt, M. C., Perez-Atayde, A., Rosenberg, A. E., Springfield, D. S., Gold, L. I., and Mankin, H. J. Expression of transforming growth factor-β (TGF-β) isoforms in osteosarcomas: TGF-β3 is related to disease progression. Cancer (Phila.), *80:* 2230–2239, 1997.
30. Callahan, J. F., Burgess, J. L., Fornbald, J. A., Gaster, L. M., Harling, J. D., Harrington, F. P., Heer, J., Kwon, C., Lehr, R., Mathur, A., Olson, B. A., Weinstock, J., and Laping, N. J. Identification of novel inhibitors of the transforming growth factor-β1 (TGF-β1) type I receptor (ALK5). J. Med. Chem., *45:* 999–1001, 2002.
31. ten Dijke, P., Yamashita, H., Ichijo, H., Franzén, P., Laiho, M., Miyazono, K., and Heldin, C-H. Characterization of type I receptors for transforming growth factor-β and activin. Science (Wash. DC), *264:* 101–104, 1994.
32. Fujii, M., Takeda, K., Imamura, T., Aoki, H., Sampath, T. K., Enomoto, S., Kawabata, M., Kato, M., Ichijo, H., and Miyazono, K. Roles of bone morphogenetic protein type I receptors and Smad proteins in osteoblast and chondroblast differentiation. Mol. Biol. Cell, *10:* 3801–3813, 1999.
33. Ota, T., Fujii, M., Sugizaki, T., Ishii, M., Miyazawa, K., Aburatani, H., and Miyazono, K. Targets of transcriptional regulation by two distinct type I receptors for transforming growth factor-β in human umbilical vein endothelial cells. J. Cell. Physiol., *193:* 299–318, 2002.
34. Ebisawa, T., Tada, K., Kitajima, I., Tojo, K., Sampath, T. K., Kawabata, M., Miyazono, K., and Imamura, T. Characterization of bone morphogenetic protein-6 signaling pathways in osteoblast differentiation. J. Cell Sci., *112:* 3519–3527, 1999.
35. Nishihara, A., Watabe, T., Imamura, T., and Miyazono, K. Functional heterogeneity of bone morphogenetic protein receptor-II mutants found in patients with primary pulmonary hypertension. Mol. Biol. Cell, *13:* 3055–3063, 2002.
36. Inman, G. J., Nicolas, F. J., Callahan, J. F., Harling, J. D., Gaster, L. M., Reith, A. D., Laping, N. J., and Hill, C. S. SB-431542 is a potent and specific inhibitor of transforming growth factor-β superfamily type I activin receptor-like kinase (ALK) receptors ALK4, ALK5, and ALK7. Mol. Pharmacol., *63:* 65–74, 2002.
37. Buchdunger, E., Zimmermann, J., Mett, H., Meyer, T., Muller, M., Druker, B. J., and Lydon, N. B. Inhibition of the Abl protein-tyrosine kinase *in vitro* and *in vivo* by a 2-phenylaminopyrimidine derivative. Cancer Res., *56:* 100–104, 1996.
38. Kovalenko, M., Gazit, A., Böhmer, A., Rorsman, C., Rönnstrand, L., Heldin, C-H., Waltenberger, J., Böhmer, F. D., and Levitzki, A. Selective platelet-derived growth factor receptor kinase blockers reverse sis-transformation. Cancer Res., *54:* 6106–6114, 1994.
39. Subramaniam, M., Oursler, M. J., Rasmussen, K., Riggs, B. L., and Spelsberg, T. C. TGF-β regulation of nuclear proto-oncogenes and *TGF-β* gene expression in normal human osteoblast-like cells. J. Cell. Biochem., *57:* 52–61, 1995.
40. Saito, T., Kinoshita, A., Yoshiura, K., Makita, Y., Wakui, K., Honke, K., Niikawa, N., and Taniguchi, N. Domain-specific mutations of a transforming growth factor (TGF)-β1 latency-associated peptide cause Camurati-Engelmann disease because of the formation of a constitutively active form of TGF-β1. J. Biol. Chem., *276:* 11469–11472, 2001.
41. Tokuyama, H., and Tokuyama, Y. Bovine colostric transforming growth factor-β-like peptide that induces growth inhibition and changes in morphology of human osteogenic sarcoma cells (MG-63). Cell Biol. Int. Rep., *13:* 251–258, 1989.
42. Pirskanen, A., Jaaskelainen, T., and Maenpaa, P. H. Effects of transforming growth factor β1 on the regulation of osteocalcin synthesis in human MG-63 osteosarcoma cells. J. Bone Miner. Res., *9:* 1635–1642, 1994.
43. Yokota, Y., and Mori, S. Role of Id family proteins in growth control. J. Cell. Physiol., *190:* 21–28, 2002.
44. Miyazaki, M., Ohashi, R., Tsuji, T., Mihara, K., Gohda, E., and Namba, M. Transforming growth factor-β1 stimulates or inhibits cell growth via down- or up-regulation of p21/Waf1. Biochem. Biophys. Res. Commun., *246:* 873–880, 1998.
45. Moustakas, A., and Kardassis, D. Regulation of the human p21/WAF1/Cip1 promoter in hepatic cells by functional interactions between Sp1 and Smad family members. Proc. Natl. Acad. Sci. USA, *95:* 6733–6738, 1998.
46. Piek, E., and Roberts, A. B. Suppressor and oncogenic roles of transforming growth factor-β and its signaling pathways in tumorigenesis. Adv. Cancer Res., *83:* 1–54, 2001.
47. Pietras, K., Rubin, K., Sjöblom, T., Buchdunger, E., Sjöquist, M., Heldin, C-H., and Östman, A. Inhibition of PDGF receptor signaling in tumor stroma enhances antitumor effect of chemotherapy. Cancer Res., *62:* 5476–5484, 2002.

THE JOURNAL OF BIOLOGICAL CHEMISTRY

Vol. 278, No. 44, Issue of October 31, pp. 43489–43495, 2003
Printed in U.S.A.

Functional Characterization of Rat Brain-specific Organic Anion Transporter (Oatp14) at the Blood-Brain Barrier

HIGH AFFINITY TRANSPORTER FOR THYROXINE*

Received for publication, June 30, 2003
Published, JBC Papers in Press, August 15, 2003, DOI 10.1074/jbc.M306933200

Daisuke Sugiyama‡, Hiroyuki Kusuhara‡, Hirokazu Taniguchi§, Shumpei Ishikawa§, Yoshitane Nozaki‡, Hiroyuki Aburatani§, and Yuichi Sugiyama‡¶

From the ‡Graduate School of Pharmaceutical Sciences, The University of Tokyo, 7-3-1 Hongo, Bunkyo-ku, Tokyo 113-0033, Japan and §Research Center for Advanced Science and Technology, The University of Tokyo, 4-6-1 Komaba, Meguro-ku, Tokyo 153-8904, Japan

Oatp14/blood-brain barrier-specific anion transporter 1 (*Slc21a14*) is a novel member of the organic anion transporting polypeptide (Oatp/OATP) family. Northern blot analysis revealed predominant expression of Oatp14 in the brain, and Western blot analysis revealed its expression in the brain capillary and choroid plexus. Immunohistochemical staining indicated that Oatp14 is expressed in the border of the brain capillary endothelial cells. When expressed in human embryonic kidney 293 cells, Oatp14 transports thyroxine (T_4; prothyroid hormone) (K_m = 0.18 μM), as well as amphipathic organic anions such as 17β estradiol-D-17β-glucuronide (K_m = 10 μM), cerivastatin (K_m = 1.3 μM), and troglitazone sulfate (K_m = 0.76 μM). The uptake of triiodothyronine (T_3), an active form produced from T_4, was significantly greater in Oatp14-expressed cells than in vector-transfected cells, but the transport activity for T_3 was ~6-fold lower that for T_4. The efflux of T_4, preloaded into the cells, from Oatp14-expressed cells was more rapid than that from vector-transfected cells (0.032 *versus* 0.006 min^{-1}). Therefore, Oatp14 can mediate a bidirectional transport of T_4. Sulfobromophthalein, taurocholate, and estrone sulfate were potent inhibitors for Oatp14, whereas digoxin, *p*-aminohippurate, or leukotriene C_4, or organic cations such as tetraethylammonium or cimetidine had no effect. The expression levels of Oatp14 mRNA and protein were up- and down-regulated under hypo- and hyperthyroid conditions, respectively. Therefore, it may be speculated that Oatp14 plays a role in maintaining the concentration of T_4 and, ultimately, T_3 in the brain by transporting T_4 from the circulating blood to the brain.

Brain capillary endothelial cells are characterized by tightly sealed cellular junctions (tight junctions) and the paucity of fenestra and pinocytotic vesicles, which prevent free exchange between brain and blood (1, 2). Therefore, the uptake of nutrients by the brain occurs through the brain capillary endothelial cells via specific transport systems (3–7). Metabolic enzymes and efflux transporters expressed in the brain capillaries facilitate the elimination of endogenous wastes and xenobiotics from the brain, and restrict their brain accumulation (3–7). Because of these characteristics, the brain capillaries are referred to as the blood-brain barrier (BBB).[1]

The organic anion transporting polypeptides (Oatps in rodents and OATPs in human) belong to the growing gene family of organic anion/prostaglandin transporters that can mediate sodium-independent membrane transport of numerous endogenous and xenobiotic amphipathic compounds (8, 9). Fourteen members of the *Oatp/OATP* gene family have been identified in rodents and humans, and they are classified within the gene superfamily of solute carriers as the *Slc21a/SLC21A* gene family (Human Gene Nomenclature Committee DataBase) (8, 9). Several members of the Oatp/OATP family have been identified in the brain (Oatp1–3 and moat1 in rodents and OATP-A in human) (10–14). Especially, in the BBB, rat Oatp2 and human OATP-A have been shown to be expressed in the plasma membrane of the brain capillary endothelial cells (15, 16). Involvement of rat Oatp2 in the uptake and efflux transport of its substrates was investigated *in vivo* (17, 18). The uptake of [D-penicillamine^{2,5}]-enkephalin (DPDPE) from the blood to the brain was determined by the brain perfusion technique in the presence and absence of Oatp2 inhibitors (17). The brain uptake of DPDPE was increased in Mdr1a (P-glycoprotein) gene knockout mice, and the uptake in Mdr1a knockout mice was inhibited by the substrates and inhibitors of rat Oatp2 such as digoxin and 17β estradiol-D-17β-glucuronide ($E_2$17βG). Vice versa, when $E_2$17βG was microinjected into the cerebral cortex, the subsequent elimination of $E_2$17βG from the brain was carrier-mediated (18), and the elimination of $E_2$17βG was completely inhibited by co-administration of taurocholate and probenecid, whereas digoxin had only a partial effect (18). Partial inhibition by digoxin suggested that additional efflux transport system(s) for $E_2$17βG, which is taurocholate- and probenecid-sensitive, is involved in the brain capillary.

Li *et al.* (19) recently identified BBB-specific anion trans-

* This work was supported by grants-in-aid from the Ministry of Health, Labor and Welfare of Japan. The costs of publication of this article were defrayed in part by the payment of page charges. This article must therefore be hereby marked "*advertisement*" in accordance with 18 U.S.C. Section 1734 solely to indicate this fact.

¶ To whom correspondence should be addressed: Dept. of Molecular Pharmacokinetics, Graduate School of Pharmaceutical Sciences, The University of Tokyo, 7-3-1 Hongo, Bunkyo-ku, Tokyo 113-0033, Japan. Tel.: 81-3-5841-4770; Fax: 81-3-5841-4766; E-mail: sugiyama@mol.f.u-tokyo.ac.jp.

[1] The abbreviations used are: BBB, blood-brain barrier; Oatp, organic anion transporting polypeptide; BSAT, BBB-specific anion transporter; HEK293, human embryonic kidney 293; CA, cholate; GCA, glycocholate; LCA, lithocholate; CDCA, chenodeoxycholate; UDCA, ursodeoxycholate; PGD_2, prostaglandin D_2; PGE_2, prostaglandin E_2; E3040, 6-hydroxy-5,7-dimethyl-2-methylamino-4-(3-pyridylmethyl) benzothiazole; PBS, phosphate-buffered saline; DPDPE, [D-penicillamine^{2,5}]-enkephalin; $E_2$17βG, 17β estradiol-D-17β-glucuronide; T_4, thyroxine; TLCS, taurolithocholate sulfate; 4-MUS, 4-methylumbelliferone sulfate; TRO-S, troglitazone sulfate; RT, reverse transcriptase; MMI, methimazole; T_3, triiodothyronine; ES, estrone sulfate; BSP, sulfobromophthalein; LT, leukotriene; D2, type 2 iodothyronine deiodinase.

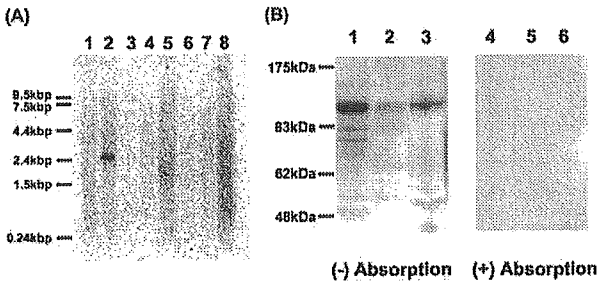

FIG. 1. **Tissue distribution of Oatp14.** *A*, Northern blotting. Commercially available rat multiple tissue Northern blots containing 2 μg of poly(A)$^+$ RNA was hybridized for 3 h using the Oatp14 fragment as a probe. *Lane 1*, heart; *lane 2*, brain; *lane 3*, spleen; *lane 4*, lung; *lane 5*, liver; *lane 6*, skeletal muscle; *lane 7*, kidney; *lane 8*, testis. *B*, Western blotting. Choroid plexus (*lanes 1* and *4*, 50 μg), brain homogenate (*lanes 2* and *5*, 50 μg), and isolated brain capillary (*lanes 3* and *6*, 50 μg) were separated by SDS-PAGE (10% separating gel). Oatp14 was detected by anti-Oatp14 polyclonal antibody.

porter 1 (BSAT1) using gene microarray techniques by comparing the gene expression profile of cDNA from the brain capillary with that from the liver and kidney. BSAT1 cDNA consisted of 2148 bp that encoded a 716-amino acid residues protein with 12 putative membrane-spanning domains. BSAT1 was highly enriched in the brain capillary compared with brain homogenate, liver, and kidney. Comparison of the cDNA sequences of BSAT1 revealed that it is the 14th member of the Oatp/OATP family (Oatp14). Although the localization at the BBB and the substrates of this isoform remain unknown, BBB-specific expression prompted us to hypothesize that Oatp14 accounts for the efflux of organic anions including $E_2 17\beta G$ via the BBB, together with Oatp2. The purpose of the present study is to characterize the substrate specificity and spectrum of inhibitors of Oatp14, as well as its tissue distribution and localization. Through this study, we found out that thyroxine (T_4) is a good substrate of Oatp14, and the expression level of Oatp14 in the BBB is affected by plasma thyroid conditions. The results of the present study suggest that Oatp14 plays an important role in regulating the concentration of T_4 in the central nervous system and in brain development.

EXPERIMENTAL PROCEDURES

Chemicals—[^{3}H]Leu-enkephalin was purchased from American Radiolabeled Chemicals (St. Louis, MO). [^{3}H]Pravastatin was kindly donated from Sankyo (Tokyo, Japan), [^{14}C]cerivastatin was from Bayer AG (Wuppertal, Germany), and [^{14}C]E3040 glucuronide and [^{14}C]E3040 sulfate were from Eisai (Tokyo, Japan). [^{3}H]Taurolithocholate sulfate (TLCS), [^{35}S]4-methylumbelliferone sulfate (4-MUS), and [^{35}S]troglitazone sulfate (TRO-S) were synthesized according to a method described previously (20, 21). The radiochemical purity of [^{3}H]TLCS, [^{35}S]4-MUS, and [^{35}S]TRO-S prepared by this method were more than 95%. Other labeled compounds were purchased from PerkinElmer Life Science. Unlabeled pravastatin, troglitazone, and its conjugated metabolites were kindly donated from Sankyo, unlabeled cerivastatin was from Bayer AG, and unlabeled E3040 glucuronide and E3040 sulfate were from Eisai. All other chemicals were commercially available, of reagent grade, and were used without any purification.

Capillary Isolation—Rat brain capillaries were isolated using a modification of the procedure of Boado *et al.* (22). All steps in the isolation procedure were carried out at 4 °C in pregassed (95% O_2-5% CO_2) solutions. Briefly, pieces of gray matter were gently homogenized in three volumes (v/w) of an artificial extracellular fluid buffer and, after addition of dextran (final concentration 15%), the homogenate was centrifuged at low speed. The resulting pellet was resuspended in Buffer B (103 mM NaCl, 25 mM $NaHCO_3$, 10 mM D-glucose, 4.7 mM KCl, 2.5 mM $CaCl_2$, 1.2 mM $MgSO_4$, 1.2 mM K_2HPO_4, and 15 mM HEPES, 1 mM sodium pyruvate, 0.5% (w/v) bovine serum albumin, pH 7.4) and then filtered through a 200-μm nylon mesh. The filtrate was passed over a column of glass beads, and after washing with Buffer B, the capillaries adhering to the beads were collected by gentle agitation.

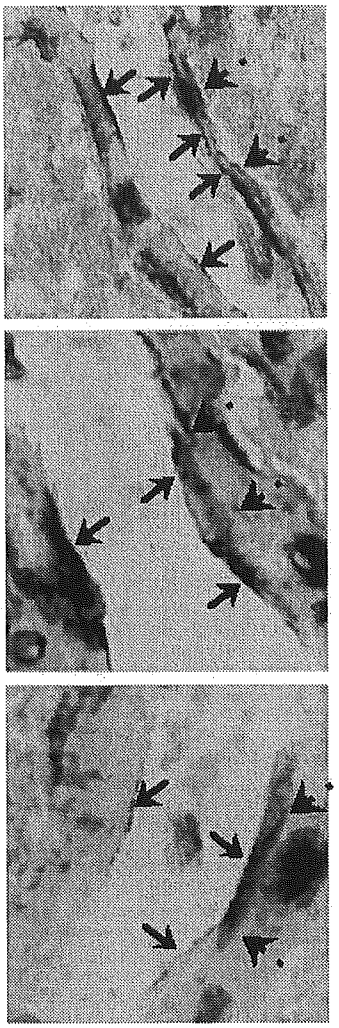

FIG. 2. **Immunohistochemical staining of Oatp14 for brain slices.** Frozen sections of rat brain were used for immunohistochemical detection with peroxidase to probe for Oatp14 with a polyclonal antibody. The *lined* and *dotted arrows* represent luminal and abluminal sides of brain capillary endothelial cells, respectively. Positive labeling was only found in the border of brain capillary endothelial cells.

Northern Blot Analysis—A commercially available hybridization blot containing poly(A)$^+$ RNA from various rat tissues (rat multi-tissue Northern blot; Clontech) was used for the Northern blot analysis. A fragment (position numbers 1–807) from Oatp14 was used as a probe, and its nucleotide sequence showed less than 60% identity with other members of the Oatp family. The master blot filter was hybridized with the ^{32}P-labeled probe at 68 °C according to manufacturer's instructions. The filter was washed finally under high stringency conditions (0.1× SSC (1× SSC = 0.15 M NaCl and 0.015 M sodium citrate)) and 0.1% SDS at 65 °C and then exposed to Fuji imaging plates (Fuji Photo Film, Kanagawa, Japan) for 3 h at room temperature and examined using an imaging analyzer (BAS 2000; Fuji Photo Film).

Western Blot Analysis—Antiserum against Oatp14 was raised in rabbits against a synthetic peptide consisting of the 17 carboxyl-terminal amino acids of Oatp14. Antiserum was purified by affinity column chromatography using the antigen and used for subsequent analyses. Choroid plexus, brain homogenate, and isolated brain capillary samples were diluted with Loading Buffer (BioLabs, Hertfordshire, United Kingdom). They were then boiled for 3 min and loaded onto an 8.5% SDS-polyacrylamide electrophoresis gel with a 3.75% stacking gel. Proteins were electroblotted onto a polyvinylidene difluoride membrane (Pall Filtran, Karlstein, Germany) using a blotter (Trans-blot; Bio-Rad) at 15 V for 1 h. The membrane was blocked with TBS-T (Tris-buffered

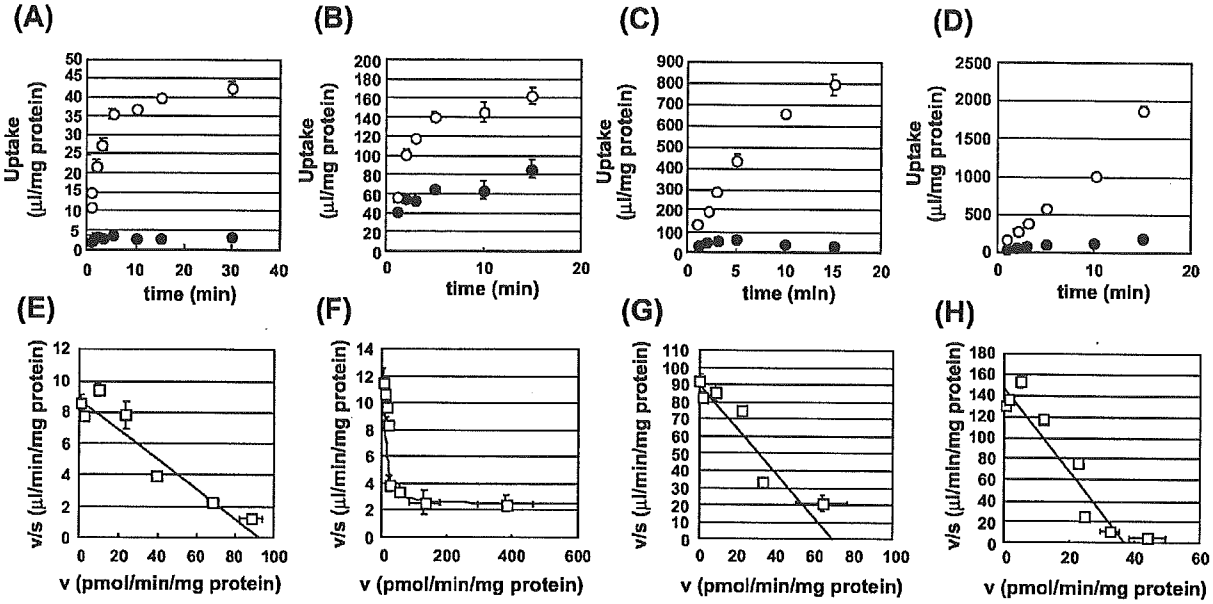

FIG. 3. **Time profiles and concentration dependence of the uptake of [^{3}H]$E_2$17βG, [^{14}C]cerivastatin, [^{35}S]TRO-S, and [^{125}I]T_4 by Oatp14-transfected HEK293 cells.** The uptake of [^{3}H]$E_2$17βG (*A* and *E*), [^{14}C]cerivastatin (*B* and *F*), [^{35}S]TRO-S (*C* and *G*), and [^{125}I]T_4 (*D* and *H*) by Oatp14-transfected HEK293 cells was examined at 37 °C. The *upper graphs* show the time profiles. *Open* and *closed circles* represent the uptake by Oatp14-transfected cells and vector-transfected cells, respectively. The *lower graphs* show the concentration dependence. Specific uptake was obtained by subtracting the uptake by vector-transfected cells from that by Oatp14-transfected cells. Each *point* represents the mean ± S.E. (n = 3).

saline containing 0.05% Tween 20) and 5% skimmed milk for 1 h at room temperature. After washing with TBS-T, the membrane was incubated with the antibodies (dilution 1:1000). The membrane was allowed to bind a horseradish peroxidase-labeled anti-rabbit IgG antibody (Amersham Biosciences) diluted 1:5000 in TBS-T for 1 h at room temperature followed by washing with TBS-T.

Immunohistochemical Study—Frozen sections from male Sprague-Dawley rats were prepared for the immunohistochemical study after fixing in acetone (−20 °C). The brain slices adhered to the glass cover slips were washed with PBS and fixed for 10 min on ice in acetone. After washing with PBS, the capillaries were permearized in 0.2% (v/v) Triton X-100 in PBS and incubated with peroxidase blocking reagent (DAKO, Carpinteria, CA) for 10 min at room temperature to block nonspecific peroxidase. Slices were incubated with anti-Oatp14 antibody (1:100) for 60 min at room temperature, washed three times with PBS, and subsequently incubated for 60 min at room temperature with the horseradish peroxidase-labeled anti-rabbit secondary antibody (Envision+ system; DAKO). The immune reaction was visualized using diaminobenzidine and then nuclei were stained with hematoxylin (DAKO). The specificity of the antibody reaction was verified by negative controls, which were incubated with polyclonal antibody that had been blocked with the antigenic peptide.

Cloning of Rat Oatp14 cDNA—Based on the nucleotide sequence reported by Li *et al.* (19) (GenBank™ accession number NM 053441), the following primers were designed to isolate Oatp14 cDNA encoding a full open reading frame of Oatp14: forward primer, 5′-ggaattccgccaccatggacacttcatccaaaga-3′ and reverse primer, 5′-ggattccttaaagtcggtctccttgc-3′. PCR was performed using cDNA prepared from rat brain as template according to the following protocol: 96 °C for 1 min, 55 °C for 1 min, and 72 °C for 2 min; 50 cycles. PCR products were subcloned to pGEM-T Easy Vector (Promega, Madison, WI) and sequenced. The nucleotide sequence of rat Oatp14 cDNA was identical as being that of BSAT1 except for one base change (A175G) resulting in a change of amino acid (T59A). However, it was confirmed that this change was not because of an error accumulated during PCR by sequencing the RT-PCR products directly.

Stable Expression of Oatp14 cDNA in HEK293 Cells—The Oatp14-cDNA was subcloned into the pcDNA3.1(+) (Invitrogen) and introduced into HEK293 cells by lipofection with FuGENE 6 (Roche Diagnostics) according to the manufacturer's protocol and were selected by culturing them in the presence of G418 sulfate (800 μg/ml; Invitrogen). HEK293 cells were grown in minimum essential medium (Invitrogen) supplemented with 10% fetal bovine serum, penicillin (100 units/ml), streptomycin (100 μg/ml), and G418 sulfate (400 μg/ml) at 37 °C with 5% CO_2 and 95% humidity. Cells were incubated for 24 h before starting the experiments with culture medium supplemented with sodium butyrate (5 mM).

Transport Study—Uptake was initiated by adding the radiolabeled ligands to the incubating buffer in the presence and absence of inhibitors after cells had been washed three times and preincubated with Krebs-Henseleit buffer (142 mM NaCl, 23.8 mM $NaHCO_3$, 4.83 mM KCl, 0.96 mM KH_2PO_4, 1.20 mM $MgSO_4$, 12.5 mM HEPES, 5 mM glucose, and 1.53 mM $CaCl_2$, adjusted to pH 7.4) at 37 °C for 15 min. For the efflux study, cells were preincubated with [^{125}I]T_4 at 37 °C for 15 min and washed three times with ice-cold Krebs-Henseleit buffer, followed by incubation in the absence of [^{125}I]T_4 with Krebs-Henseleit buffer at 37 °C. The uptake and efflux were terminated at designed times by adding ice-cold Krebs-Henseleit buffer. The radioactivity associated with the cells and medium specimens was determined in a liquid scintillation counter. The remaining aliquots of cell lysates were used to determine protein concentrations by the method of Lowry (23) with bovine serum albumin as a standard. Ligand uptake is given as the cell-to-medium concentration ratio determined as the amount of ligand associated with the cells divided by the medium concentration. Specific uptake was obtained by subtracting the uptake by vector-transfected cells from that by Oatp14-expressed cells.

Kinetic Analyses—Kinetic parameters were obtained from the following Michaelis-Menten equation, $v = V_{max}S/(K_m + S)$, where v is the uptake rate of the substrate (pmol/min/mg protein), S is the substrate concentration in the medium (μM), K_m is the Michaelis-Menten constant (μM), and V_{max} is the maximum uptake rate (pmol/min/mg protein). To obtain the kinetic parameters, the equation was fitted to the initial uptake velocity. The experimental data were fitted to the equation by nonlinear regression analysis with weighting as the reciprocal of the observed values, and the Damping Gauss Newton Method algorithm was used for fitting. Inhibition constants (K_i) for Oatp14-mediated transport were calculated assuming competitive inhibition.

Production of Hyperthyroid and Hypothyroid Conditions—Male Sprague-Dawley rats, weighing 200–220 g, were purchased from Japan SLC (Shizuoka, Japan). Rats had free access to food and water at all times during the study. Production of hyperthyroid and hypothyroid conditions involved a modification of the procedure of Burmeister *et al.* (24). Hypothyroidism was induced by the addition of 0.05% methimazole (MMI), an inhibitor for thyroid hormone synthesis in the thyroid gland, to the drinking water or thyroidectomy. Hypothyroidism was assessed clinically by failure to gain weight at the expected rate and

TABLE I
Substrate specificity of Oatp14

Oatp14-expressed and vector-transfected HEK293 cells were grown to confluence. After 24 h of incubation in culture medium including 5 mM sodium butyrate, uptake was examined in Krebs-Henseleit buffer.

Substrates	Oatp14	pcDNA	Ratio, Oatp14/pcDNA
	μl/mg protein/15 min		
CA	5.66 ± 0.30	5.24 ± 0.43	1.1 ± 0.1
GCA	18.7 ± 2.3	15.7 ± 1.6	1.2 ± 0.2
TCA	8.09 ± 0.52	6.06 ± 0.10	1.3 ± 0.1[a]
LCA	576 ± 6	535 ± 18	1.1 ± 0.0
CDCA	65.7 ± 6.7	84.1 ± 11.5	0.8 ± 0.1
UDCA	10.5 ± 0.1	9.71 ± 0.35	1.1 ± 0.0
TLCS	61.5 ± 1.9	43.7 ± 1.7	1.4 ± 0.1
Estradiol	204 ± 4	186 ± 13	1.1 ± 0.1
Testosterone	52.3 ± 1.5	39.2 ± 1.4	1.3 ± 0.1[b]
Dihydrotestosterone	147 ± 15	106 ± 5	1.4 ± 0.2[b]
Corticosterone	24.7 ± 1.5	20.9 ± 0.5	1.2 ± 0.1
Estrone	303 ± 15	248 ± 6	1.2 ± 0.1[a]
DHEAS	9.68 ± 0.24	7.72 ± 0.48	1.3 ± 0.1[a]
Estrone-sulfate	11.1 ± 0.8	6.3 ± 0.1	1.7 ± 0.1[a]
$E_2$17βG	50.1 ± 4.7	2.4 ± 0.2	21.2 ± 2.9[b]
LTC4	14.5 ± 0.6	13.4 ± 0.1	1.1 ± 0.0[b]
LTD4	19.6 ± 0.8	18.0 ± 2.0	1.1 ± 0.1
LTE4	30.5 ± 1.3	26.0 ± 0.9	1.2 ± 0.1[a]
PGD2	3.50 ± 0.15	3.61 ± 0.12	1.0 ± 0.1
PGE2	6.99 ± 0.46	5.80 ± 0.24	1.2 ± 0.1
Leu-Enkephalin	54.2 ± 2.9	43.3 ± 2.5	1.3 ± 0.1[a]
CCK-8	2.58 ± 0.21	1.81 ± 0.13	1.4 ± 0.2[a]
T3	951 ± 16	733 ± 4	1.3 ± 0.0[b]
Reverse T3	1397 ± 79	71 ± 5	19.7 ± 1.7[b]
T4	1456 ± 10	124 ± 3	11.8 ± 0.3[b]
Ketoprofen	9.53 ± 0.42	6.91 ± 0.26	1.4 ± 0.1[b]
Ibuprofen	3.18 ± 0.11	3.99 ± 1.18	0.8 ± 0.2
Indomethacin	31.3 ± 0.9	34.3 ± 2.0	0.9 ± 0.1
Benzylpenicillin	5.76 ± 0.47	5.45 ± 0.12	1.1 ± 0.1
OchratoxinA	8.58 ± 1.29	5.81 ± 0.14	1.5 ± 0.2[b]
Qunidine	1390 ± 34	1274 ± 150	1.1 ± 0.1
Cerivastatin	105 ± 2	33 ± 1	3.1 ± 0.1[b]
Pravastatin	5.62 ± 0.38	3.50 ± 0.75	1.6 ± 0.4[a]
Digoxin	8.70 ± 0.13	9.96 ± 0.22	0.9 ± 0.0
E3040	106 ± 3	93 ± 5	1.1 ± 0.1
E3040G	10.7 ± 1.0	2.12 ± 0.22	5.1 ± 0.7[a]
E3040S	4.78 ± 0.35	1.69 ± 0.26	2.8 ± 0.5[b]
4MUS	1.82 ± 0.35	0.90 ± 0.03	2.0 ± 0.1[b]
Troglitazone-sulfate	64.1 ± 14.3	8.4 ± 0.4	7.6 ± 1.7[b]

[a] Statistically significant uptake is indicated. $p < 0.05$.
[b] Statistically significant uptake is indicated. $p < 0.01$.

TABLE II
K_m, V_{max} and V_{max}/K_m values for Oatp14

The K_m and V_{max} values were determined by nonlinear regression analysis using data shown in Fig. 3.

Substrate	K_m	V_{max}	V_{max}/K_m
	μM	*pmol/min/mg protein*	*μl/min/mg protein*
$E_2$17βG	10.7 ± 1.6	93.4 ± 10.4	8.73 ± 1.63
Cerivastatin	1.34 ± 0.25	14.5 ± 2.2	10.8 ± 2.6
TRO-S	0.76 ± 0.09	69.0 ± 6.7	91.3 ± 14.2
T4	0.18 ± 0.03	32.1 ± 2.5	147 ± 14

could be observed within 2 weeks of the beginning MMI treatment and within 1 week after thyroidectomy. Hyperthyrodism was produced by giving L-T3 (50 μg/100 g body weight, subcutaneously, daily) 4 days before capillary isolation.

RESULTS

Tissue Distribution of Oatp14—The expression of Oatp14 mRNA in rat tissues was investigated by Northern blot analysis (Fig. 1*A*). A band was detected at 2.6 kbp, predominantly in the brain. No hybridization signals were detected in mRNA isolated from other tissues, including the heart, spleen, lung, liver, skeletal muscle, kidney, and testis.

Immunoblot and Immunohistochemical Staining of Oatp14—The expression of Oatp14 in the choroid plexus, brain homogenate, and brain capillary was examined by Western blot analysis (Fig. 1*B*). Immunoreactive protein was detected at ~90 kDa in the choroid plexus, brain homogenate, and brain capillary. These bands were abolished when preabsorbed polyclonal antibody for Oatp14 was used, suggesting that the positive bands were specific for the antigen peptide.

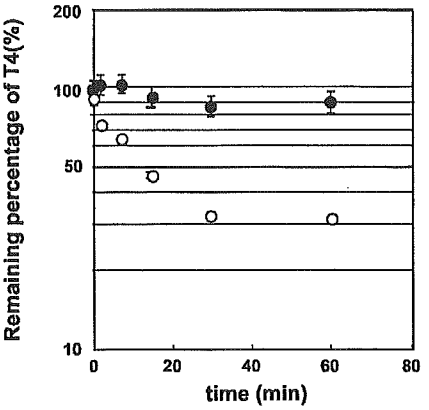

FIG. 4. **Time profiles of the efflux of [^{125}I]T_4 from Oatp14-transfected HEK293 cells.** The efflux of preloaded [^{125}I]T_4 from Oatp14-transfected HEK293 cells was examined at 37 °C. *Open* and *closed circles* represent the efflux from Oatp14- and vector-transfected cells, respectively. Each *point* represents the mean ± S.E. (n = 3).

To investigate the localization of Oatp14 in brain capillary endothelial cells, immunohistochemical staining was carried out using anti-Oatp14 polyclonal antibody (Fig. 2). Positive signals for anti-Oatp14 polyclonal antibody were detected in brain capillary endothelial cells. The signals were detected along the plasma membrane of brain capillary endothelial cells. The signal was abolished by preincubating the polyclonal antibody of Oatp14 with antigen (data not shown).

Transport Properties of Oatp14—Fig. 3 shows the time profiles of the uptake of [^{3}H]$E_2$17βG (*A*), [^{14}C]cerivastatin (*B*), [^{35}S]TRO-S (*C*), and [^{125}I]T_4 (*D*) by Oatp14-expressed HEK293 cells and vector-transfected HEK293 cells. Their uptake by Oatp14-expressed cells is markedly greater than that by vector-transfected cells. This Oatp14-mediated uptake showed saturation kinetics and followed the Michaelis-Menten equation (Fig. 3, *E-H*). The kinetic parameters for the uptake by Oatp14 were determined by nonlinear regression analysis and summarized in Table I. The uptake of various organic anions by Oatp14 was investigated, and the results are summarized in Table II. The uptake of [^{14}C]E3040 glucuronide, [^{14}C]E3040 sulfate, [^{14}C]4-MUS, and [^{125}I]reverse T_3 by Oatp14-expressed cells was significantly greater compared with that by vector-transfected (Table II). Although the triiodothyronine (T_3) uptake by Oatp14-expressed cells was significantly greater than that by vector-transfected cells, the Oatp14-mediated uptake for T_3 was ~6-fold smaller than that of T_4 and reverse T_3 by Oatp14 (Table II). The difference in the uptake of [^{3}H]taurocholate, [^{3}H]TLCS, [^{3}H]testosterone, [^{3}H]dihydrotestosterone, [^{3}H]estrone, [^{3}H]estrone sulfate (ES), [^{3}H]dehydroepiandrosterone sulfate, [^{3}H]leukotriene E_4 (LTE_4), [^{3}H]Leu-enkephalin, [^{3}H]cholecystokinin-octapeptide (CCK-8), [^{125}I]T_3, [^{3}H]pravastatin, [^{3}H]ketoprofen, and [^{3}H]ochratoxin A was statistically significant between Oatp14-expressed and vector-transfected cells, although the rates of uptake were very low (Table II).

To investigate whether Oatp14 can mediate bidirectional transport, cells were preloaded with [^{125}I]T_4 for 15 min followed by incubation in the absence of [^{125}I]T_4. The radioactivity associated with cell specimens was rapidly reduced in Oatp14-expressed HEK293 cells compared with that in vector-trans-